NanoImpact 19 (2020) 100235

Contents lists available at ScienceDirect

NanoImpact

journal homepage: www.elsevier.com/locate/nanoimpact

Toxicity evaluation following pulmonary exposure to an as-manufactured dispersed boron nitride nanotube (BNNT) material *in vivo*

Xing Xin[a], Mark Barger[a], Katherine A. Roach[a], Lauren Bowers[a], Aleksandr B. Stefaniak[b], Vamsi Kodali[a], Eric Glassford[c], Kevin L. Dunn[c], Kevin H. Dunn[c], Michael Wolfarth[a], Sherri Friend[a], Stephen S. Leonard[a], Michael Kashon[a], Dale W. Porter[a], Aaron Erdely[a], Jenny R. Roberts[a,*]

[a] National Institute for Occupational Safety and Health, Health Effects Laboratory Division, 1095 Willowdale Rd., Morgantown, WV 26505, United States of America
[b] National Institute for Occupational Safety and Health, Respiratory Health Division, 1095 Willowdale Rd., Morgantown, WV 26505, United States of America
[c] National Institute for Occupational Safety and Health, Division of Field Studies and Engineering, 5555 Ridge Ave., Cincinnati, OH 45213, United States of America

ARTICLE INFO

Editor: Philip Demokritou

Keywords:
Boron nitride nanotubes
Pulmonary toxicity
Inflammation
Pathology
In vivo

ABSTRACT

Boron nitride nanotubes (BNNT) are multi-walled nanotubes composed of hexagonal B—N bonds and possess many unique physical and chemical properties, creating a rapidly expanding market for this newly emerging nanomaterial which is still primarily in the research and development stage. The shape and high aspect ratio give rise to concern for the potential toxicity that may be associated with pulmonary exposure, especially in an occupational setting. The goal of this study was to assess lung toxicity using an *in vivo* time course model. The sample was manufactured to be 5 nm wide and up to 200 μm long, with ~50% purity covalently bound with hexagonal boron nitride (hBN) in the sample. Following preparation for *in vivo* studies, sonication of the material disrupted the longer tubes in the complex and the size distribution in dispersion medium (DM) of the structures was 13–23 nm in diameter and 0.6–1.6 μm in length. Male C57BL/6 J mice were exposed to 4 or 40 μg of BNNT or DM (vehicle control) by a single oropharyngeal aspiration. Pulmonary and systemic toxicity were investigated at 4 h, 1 d, 7 d, 1 mo and 2 mo post-exposure. Bronchoalveolar lavage (BAL) studies determined pulmonary inflammation (neutrophil influx) and cytotoxicity (lactate dehydrogenase activity) occurred at early time points and peaked at 7 d post-exposure in the high dose group. Histopathological analysis showed a minimal level of inflammatory cell infiltration in the high dose group with resolution over time and no fibrosis, and lung clearance analysis showed ~50% of the material cleared over the time course. The expression of inflammatory- and acute phase response-associated genes in the lung and liver were significantly increased by the high dose at 4 h and 1 d post-exposure. The increases in lung gene expression of *Cxcl2*, *Ccl2*, *Il6*, *Ccl22*, *Ccl11*, and *Spp1* were significant up to 2 mo but decreased with time. The low dose exposure did not result in significant changes in any

Abbreviations: APC, allophycocyanin; AL, alveolar lumen; AM, alveolar macrophages; AS, alveolar septae; ANOVA, analysis of variance; BNNT, boron nitride nanotubes; BV, brilliant violet; BL, bronchiolar lumen; BAL, bronchoalveolar lavage; BET, Brunauer, Emmett and Teller; CNT, carbon nanotubes; CD, cluster of differentiation; CMD, count median diameter; DNA, deoxyribonucleic acid; DPPC, 1,2-dipalmitoyl-sn-glycero-3-phosphotidyl; DM, dispersion medium; DLS, dynamic light scattering; EDM, enhanced darkfield microscopy; LIX, epithelial-derived neutrophil-activating peptide 78; EDTA, ethylenediaminetetraacetic acid; FESEM, field emission scanning electron microscopy; FITC, fluorescein isothiocyanate; GSD, geometric standard deviation; G-CSF, Granulocyte-Colony Stimulating Factor; GM-CSF, Granulocyte-Macrophage-Colony Stimulating Factor; H&E, hematoxylin and eosin; hBN, hexagonal boron nitride; IFN, Interferon; ICP-AES, inductively-coupled plasma-emission spectroscopy; IP, interferon-gamma-inducible protein; IL, interleukin; LDH, lactate dehydrogenase; LIF, Leukemia Inhibitory Factor; M-CSF, Macrophage-Colony Stimulating Factor; MDC, macrophage-derived chemokine; MIP, macrophage inflammatory protein; MLN, mediastinal lymph node; MT, metallothionein; ML, mixed leukocyte infiltration; MCP, monocyte chemotactic protein; MIG, Monocyte Induced by Gamma Interferon; MWCNT, multi-walled carbon nanotubes; MPPD, Multiple-Path Particle Dosimetry Model; NK, natural killer; KC, Neutrophil Activating Protein CXCL1; NAD+, nicotinamide adenine dinucleotide; OPN, osteopontin; PerCP, peridinin-chlorophyll-protein; PV/PB, perivascular/peribronchiolar; PBS, phosphate-buffered saline; PE, phycoeryhtrin; PCR, polymerase chain reaction; PMN, polymorphonuclear cells; RANTES, regulated on activation-normal T cell expressed and secreted; RNA, ribonucleic acid; SPP, secreted phosphoprotein; SAA, serum amyloid A; SSA, specific surface area; TEM, transmission electron microscopy; TNF, Tumor Necrosis Factor; VEGF, vascular endothelial growth factor; WBC, white blood cells

* Corresponding author at: CDC/NIOSH/HELD/ACIB, 1095 Willowdale Rd., MS4020/L3407, Morgantown, WV 26505, United States of America.
E-mail addresses: wvq1@cdc.gov (K.A. Roach), mju3@cdc.gov (L. Bowers), boq9@cdc.gov (A.B. Stefaniak), ywu0@cdc.gov (V. Kodali), yxx7@cdc.gov (E. Glassford), kgd8@cdc.gov (K.L. Dunn), kfd5@cdc.gov (K.H. Dunn), mgz1@cdc.gov (M. Wolfarth), shf8@cdc.gov (S. Friend), sel5@cdc.gov (S.S. Leonard), mqk1@cdc.gov (M. Kashon), dhp7@cdc.gov (D.W. Porter), efi4@cdc.gov (A. Erdely), jur6@cdc.gov (J.R. Roberts).

https://doi.org/10.1016/j.impact.2020.100235
Received 25 March 2020; Received in revised form 18 June 2020; Accepted 23 June 2020
Available online 29 June 2020

toxicological parameters measured. In summary, the BNNT-hBN sample used in this study caused acute pulmonary inflammation and injury at the higher dose, which peaked by 7 d post-exposure and showed resolution over time. Further studies are needed to determine if physicochemical properties and purity will impact the toxicity profile of BNNT and to investigate the underlying mechanisms of BNNT toxicity.

1. Introduction

Boron Nitride nanotubes (BNNT) were first synthesized in 1995, as structural analogs of carbon nanotubes (CNTs) where C—C bonds are substituted by alternating B and N atoms. BNNT are high aspect ratio multi-walled nanotubes with 4–5 layers of hexagonal B—N in tube formation that can range in lengths from a few nanometers up to 200 μm, and in diameter from 2 to 200 nm (Chopra et al., 1995; Jakubinek et al., 2019; Smith et al., 2009; Tiano et al., 2014). The first commercial BNNT were made available in 2014 (Jakubinek et al., 2019). BNNT are currently produced primarily for research and diagnostic purposes and are considered an emerging material of great interest due to their unique combination of physical and chemical properties. These properties include high thermal stability and conductivity, anti-oxidation ability, high hydrogen storage capacity, radiation absorption, electrical insulation, super hydrophobicity, chemical inertness and surface polarization (Golberg et al., 2007; Smith et al., 2009; Tiano et al., 2014), and in some aspects are superior to the multi-walled carbon nanotubes (MWCNT). They possess a constant band gap of ~5.5 eV, resulting in superior insulating properties and thermal stability (Zhi et al., 2005). Due to these properties, BNNT offer advantages in applications that require superior neutron absorption, piezoelectricity, and visual transparency (Tiano et al., 2014). Combinations of these properties make BNNT an attractive material for use in wide-ranging markets from the aerospace industry to automotive and defense industries to the biomedical fields, including but not limited to use in ceramic and polymer composites, aerospace components, batteries, radiation shielding, piezoelectric systems for sensors and robotics in energy harvesting and satellites, fire retardant cabling, and potential biomedical applications in drug delivery, tissue engineering, and biosensors (Kim et al., 2018; Lee et al., 2016). Production estimates are currently not available as many of the application as are still in the research stage; however, with the wide range of potential applications, the production of BNNT is likely to increase significantly which may lead to a potential risk for pulmonary exposure to the material, particularly in terms of occupational routes of exposure in the workplace, where the material is handled in powder form prior to incorporation into a final product. To date, very little is known regarding the *in vivo* toxicity of BNNT, particularly following respiratory exposure. There is currently only one *in vivo* pulmonary study available which demonstrated that BNNT induced acute toxicity in a mouse model at 24 h following oropharyngeal aspiration (Kodali et al., 2017). Other *in vivo* toxicity studies that investigated the biocompatibility of BNNT in relationship to biomedical applications found no adverse effects of BNNT; however, these studies either used different species, such as freshwater planarians (Salvetti et al., 2015), or examined different routes of exposure such as intravenous injection in rabbits (Ciofani et al., 2012, 2013). The reported results from *in vitro* toxicity studies are contradictory. Some of the studies indicated that BNNT are nontoxic (Chen et al., 2009; Ciofani et al., 2010), while others demonstrated that BNNT are cytotoxic, can induce oxidative stress, and cause DNA damage on specific cell types (Cal and Bucurgat, 2019; Horvath et al., 2011; Kodali et al., 2017). The disputing results may be due to different commercial BNNT products, different surface coating of the BNNT particle, different cell types, or different exposure time. Taken together, these studies indicate that further investigation into the toxicity of BNNT is required, particularly related to potential occupational exposures.

The goal of the present study was to explore the pulmonary toxicity following respiratory exposure to a commercially available BNNT sample. The sample evaluated in this study, was provided in conjunction with an exposure assessment at a manufacturing facility and contained approximately 50% nanotubes, with hexagonal BN (hBN) and boron covalently bound to the nanotubes. Boron compounds in bulk form have been associated with nose, throat, and eye irritation that has been shown to resolve with reduction in exposures (ATSDR, 2010). Regulatory recommendations exist for several boron-based compounds including borates, borax, boron fluoride, and boron tribromide with time-weighted average exposures set at 1 mg/m^3, 5 mg/m^3, 3 mg/m^3, and 10 mg/m^3, respectively (NIOSH, 2007). Effects of exposure to boron compounds in humans and mammals have been observed, including lung irritation, cough and decreased lung function; however, these effects only manifest at concentrations that exceed the recommended limits mentioned above (EPA, 2004). Therefore, based on the low level of toxicity associated with boron compounds, we hypothesized that the exposure to this complex material would not produce persistent pathology in the lung following respiratory exposure. To this end, following material characterization, and *in vivo* time course study was conducted following pulmonary exposure to the BNNT sample in mice.

2. Methods

2.1. Particle characterization and dispersion

The BNNT sample used in this study was synthesized and provided by BNNT, LLC (Smith et al., 2009). This facility is a primary manufacturer of the material. The BNNT were originally manufactured to be 5 nm wide and up to 200 μm long. The synthesis processes used for this BNNT sample resulted in a sample that contains ~50% BNNT which is hBN layered into a multi-walled tube formation with the remaining portion of the sample composed of primarily hBN by-product, as well as boron and amorphous boron nitride, covalently bound in the sample. This is referred to as the as-produced BNNT sample. Field emission scanning electron microscopy (FESEM, Hitachi Model S-4800, Japan) imaging was used to visualize and verify size of the particle in the dry powder form. The Brunauer, Emmett and Teller (BET) surface area of BNNT sample was measured using nitrogen gas adsorption (ASAP2020, Micromeritics, Norcross, GA). A value of 1.62×10^{-19} m^2 was used for the molecular cross-sectional area of N_2 at 77 K. The BET surface area was calculated from at least seven adsorption points in the range $p/p^0 = 0.01$ to 0.35 (ASTM, 2002). Skeletal density was measured by helium pycnometry (AcuPyc II 1345, Micromeritics, Norcross, GA) in accordance with standard method ASTM B923 (ASTM, 2008).

For *in vivo* studies, aspiration requires that the nanoparticles be suspended in a compatible vehicle for delivery to the animals. The BNNT sample was weighed and suspended in 100% ethanol and sonicated for 10 min in a cup-horn sonicator to optimize the dispersion. Samples were then dried to remove the ethanol, and the BNNT particles were sized by point count method from FESEM images. The dried BNNT sample was suspended in well-characterized dispersion medium [DM; 0.6 mg/ml mouse serum albumin + 0.01 mg/ml 1,2-dipalmitoyl-sn-glycero-3-phosphotidyl (DPPC) in phosphate-buffered saline (PBS) without calcium and magnesium] (Porter et al., 2008) followed by a second cup-horn sonication for 5 min at a concentration of 0.8 mg/ml (equivalent to the high dose, 40 μg particle/50 μl DM). The energy setting of the sonication process delivered a total of 2100 J over the course of the two sonications at a delivery rate of 2.33 J/s. The low dose (4 μg/50 μl) of samples was prepared by diluting the high dose 1: 10

following sonication. The DM has been shown to be non-toxic itself, and to not mask toxicity of particles. Particle dispersion in DM was made on the day of use for both characterization and *in vivo* studies.

Hydrodynamic diameter (agglomerate size) was measured by dynamic light scattering (DLS; Microtrac Inc., San Diego, CA) on 10 separate sample preparations that prepared identically to the high dose in DM that was delivered to the mice. Zeta potential (agglomerate charge) was determined by electrophoretic mobility using a Malvern Zetasizer Nano ZS90 (Worcestershire, UK) equipped with a 633 nm laser at a 90° scattering angle. A stock solution of BNNT sample in DM (1 mg/ml) was sonicated using a 3 mm probe tip for 5 min and further diluted using fresh DM. All measurements were performed at 25 °C based on PBS, the major constituent of DM. Samples were equilibrated inside the instrument for 2 min, and five measurements, each consisting of five runs, were recorded. The delivered energy in this preparation was 1650 J which was 450 J less than that of the preparations for DLS measures and exposures, and this should be taken into consideration as the dispersion may be slightly different from those used in the exposures.

Surface reactivity of the BNNT in DM was measured by electron paramagnetic resonance. Briefly, generation of hydroxyl radicals on the particle surface as an indicator of surface reactivity was evaluated using an EMX spectrometer (Bruker Instruments Inc., Billerica, MA) and a flat cell assembly (Janzen and Blackburn, 1968). For this study, hydroxyl radical was generated from a Fenton-like reaction system after the BNNT sample was prepared in DM identically to the preparation for animal exposures (at a dose equivalent to the high dose used in this study) combined with H_2O_2 [1 mM] in the presence of 100 mM of the spin trap 5,5-dimethyl-1-pyrroline N-oxide (DMPO) and PBS to a final volume of 1 ml. The reaction was also performed from the DM control and a positive control material, copper nanoparticles, at the same concentration. Reactions were allowed to incubate 3 min at room temperature before measurement. Signal intensity of the spin adduct, which corresponds to the amount of a given radical species, was determined by integration of the characteristic wave form for that radical. The wave form was then measured and quantified and compared to the positive control.

2.2. Animals and in vivo exposure

Male C57BL6 J mice, ~8 weeks of age, were obtained from Jackson Laboratory (Bar Harbor, ME) for use in this study. All mice were housed in polycarbonate ventilated cages with HEPA-filtered air in the AAALAC-international accredited National Institute for Occupational Safety and Health (NIOSH) Animal Facility, and provided food (Harlan Teklad Rodent Diet 7913, Indianapolis, IN) and tap water *ad libitum* in a controlled humidity and temperature environment with a 12 h light/dark cycle. Animals were allowed to acclimate for 1 week in the facility prior to use in the study. All procedures in the study comply with the ethical standards set forth by the Animal Welfare Act (enforced by the United States Department of Agriculture) and the Office of Laboratory Animal Welfare (OLAW). The studies were approved by the CDC-Morgantown Institutional Animal Care and Use Committee (Public Health Services Assurance Number D16-00687) in accordance with an approved institutional animal protocol.

A time course study in mice was conducted to evaluate pulmonary and extrapulmonary toxicity following lung exposure to the BNNT sample. On 0 d, two sets of male C57BL/6 J mice were exposed by a single oropharyngeal aspiration to 4 or 40 μg of the BNNT sample in DM, or DM alone (vehicle control) in a volume of 50 μl. Mice were humanely euthanized with an overdose of sodium pentobarbital euthanizing solution (100–300 mg/kg bw, Fatal Plus, Vortech Pharmaceuticals, Dearborn, MI) at 4 h, 1 d, 7 d, 1 mo, and 2 mo post-exposure. Immediately following euthanasia blood was collected from the inferior vena cava for hemocytology and serum was retained for analyses. Bronchoalveolar lavage (BAL) was performed on one set of mice from each group to collect fluid and cells (n = 8 per group per time point) for pulmonary toxicological analyses. Lymphocytes from the mediastinal lymph node and spleen were isolated and differentiated. In the second set of mice (n = 8 per group per time point), the left lung was ligated and frozen in liquid nitrogen for RNA analysis while the right lungs were fixed, sectioned, and stained for histopathology. A liver section for RNA isolation was snap-frozen in RNA-free tubes in liquid nitrogen at the time of tissue collection. To evaluate pulmonary clearance of particles, a third set of mice was exposed to the BNNT sample at a dose of 40 μg, and boron was measured in lungs that were removed following euthanasia at 1 d, 7 d, 1 mo, and 2 mo.

2.3. BAL cellular and fluid analysis

2.3.1. Lung lavage

In a separate group of mice, BAL was performed on the lung in order to obtain pulmonary cells and fluid for analysis of indicators of lung injury, inflammation, and cellular activity (n = 8 per group per time point). Following euthanasia, the trachea was cannulated, the chest cavity was opened, and BAL was performed on the whole lungs. The first lavage was obtained by instilling the lung with 0.6 ml PBS, massaging for 30 s, and withdrawing. This concentrated aliquot was retained, kept separately, and was designated as the first fraction of BAL. The following aliquots were 0.6 ml in volume, instilled once with light massaging, withdrawn, and combined until a 2.4 ml volume was obtained, presenting the second fraction of BAL. For each animal, both lavage fractions were centrifuged (500*g*, 10 min, 4 °C) and the cell pellets from both fractions were combined and resuspended in 1 ml of PBS for cell counts and differentials. The acellular fraction of BAL fluid from the first lavage was retained for analysis of lactate dehydrogenase (LDH) activity and protein content.

2.3.2. BAL cell differentiation

The total numbers of BALC cells collected from mice were counted using a Coulter Multisizer 4 (Coulter Electronics, Hialeah FL). Cell differentials were performed to determine the total number of alveolar macrophages (AM), neutrophils, and eosinophils (n = 8 per group per time point). Briefly, 10^5 cells from each mouse were spun down onto slides with a Cytospin 3 centrifuge (Shandon Life Sciences International, Cheshire, England) and labeled with Leukostat stain (Fisher Scientific, Pittsburgh PA) to determine the cell phenotypes. Two hundred cells per slide were counted, and the percentages of AM, neutrophils, and eosinophils were multiplied by the total number of cells to calculate the total number of each cell type. Total lymphocytes in BAL were determined by flow cytometry as described below.

2.3.3. Lactate dehydrogenase (LDH) activity

The level of LDH activity in BAL fluid was measured in the first fraction BAL fluid supernatant at each time point after exposure to evaluate cytotoxicity as an indicator of lung injury. Measurements of LDH activity were obtained using a Cobas C111 analyzer (Roche Diagnostic Systems, Montclair IN). LDH activity was quantified by detection of the oxidation of lactate coupled to the reduction of NAD^+ at 340 nm (n = 8 per group per time point).

2.3.4. BAL fluid protein analysis

A panel of 32 proteins involved in inflammatory, irritant and immune responses were measured at each time point after exposure in the BAL fluid of mice treated with DM or BNNT by multiplex array (n = 6 per group per time point) (Eve Technologies, Alberta, CA). Eotaxin, Granulocyte-Colony Stimulating Factor (G-CSF), Granulocyte-Macrophage Colony Stimulating Factor (GM-CSF), Interferon(IFN)γ, Interleukin (IL)-1α, IL-1β, IL-2, IL-3, IL-4, IL-5, IL-6, IL-7, IL-9, IL-10, IL-12 (p40), IL-12(p70), IL-13, IL-15, IL-17, IP-10 (IFN-γ-inducible protein (IP)-10), Neutrophil Activating Protein CXCL1 (KC), Leukemia Inhibitory Factor (LIF), Epithelial-Derived Neutrophil-Activating Peptide 78 (LIX), Macrophage Chemotactic Protein (MCP)-1,

Macrophage-Colony Stimulating Factor (M-CSF), Monocyte Induced by Gamma Interferon (MIG), Monocyte Inflammatory Protein (MIP)-1α, MIP-1β, MIP-2, regulated on activation, normal T-cell expressed and secreted (RANTES), Tumor Necrosis Factor (TNF)α, and vascular endothelial growth factor (VEGF) were assessed.

2.4. Lymphocyte phenotypic quantification of BAL cells, mediastinal lymph node (MLN), and spleen

In addition to BAL cells, lung-associated lymph nodes (mediastinal nodes) and spleen were collected to enumerate lymphocyte phenotype as an index of local and systemic immune response. Lymphocyte populations in BAL cells, MLN, and spleen were differentially assessed by multicolor flow cytometry analysis (n = 8 per group per time point). Single cell suspensions were obtained from BAL or by homogenizing the MLN or spleen manually between frosted microscope slides. Concentrations of cells from each tissue were determined using a coulter counter, as described for enumeration of BAL cells. For flow cytometry staining, 500,000 cells from each tissue were suspended in staining buffer (PBS + 1% bovine serum albumin + 0.1% sodium azide) containing Fc receptor-blocking anti-mouse CD16/32 (1 μg/500,000 cells; BD Biosciences; San Diego, CA) to reduce non-specific antibody binding. Cells were incubated for 5 min, washed, and re-suspended in staining buffer containing a panel of fluorochrome-conjugated antibodies (final concentration, 1–10 μg/ml) to allow for differentiation of CD4+ T-cells, CD8+ T-cells, B-cells, and NK Cells. BAL, lymph node, and spleen cells were stained with CD2-BV605 (clone RM2-5), CD3-APC (clone 145-2C11), CD4-FITC (clone GK1.5), CD8-PE (clone 53-6.7), CD44-APC-R700 (clone IM7), CD45-PerCP (clone 30-F11), CD45R(B220)-PE-Cy7 (RA3-6B2), and CD86-BV421(clone GL1) (all from BD Biosciences; San Diego, CA). Cells were incubated for 30 min, washed, and fixed in 100 μl Cytofix Buffer (BD Biosciences, San Diego, CA). Single-stain and fluorescence minus one compensation controls were prepared using UltraComp eBeads (eBioscience; San Diego, CA) and corresponding cell types, and unstained lung cells were used to compensate for background autofluorescence. For each sample, 100,000 events were recorded on an LSR II flow cytometer (BD Biosciences, San Diego, CA). In all analysis, doublet exclusion was performed, and cellular populations were gated using FSC-A x SSC-A parameters prior to subsequent analysis. All data analysis was performed using FlowJo 7.6.5. Software (TreeStar Inc.; Ashland, OR).

2.5. White blood cell differentials

Blood was collected from the inferior vena cava in mice prior to BAL. A fraction of whole blood was collected into EDTA tubes for differential analysis of white blood cells (neutrophils, lymphocytes, monocytes, basophils, and eosinophils) using a ProCyte Dx (n = 6–8 per group per time point) (IDEXX Laboratories, Westbrook, ME).

2.6. Histopathology, macrophage uptake and pulmonary clearance

The right lung lobes (apical, cardiac, and diaphragmatic) from another set of mice were fixed with 10% neutral buffered formalin by airway pressure fixation under 30 cm water pressure to total lung capacity for 15 min. All three lobes were embedded in paraffin, sectioned onto slides, and stained with hematoxylin and eosin (H&E) for parameters of injury and inflammation. Stained slides from DM control, low, and high dose of BNNT mice were evaluated at each time point of 1 d, 7 d, 1 mo and 2 mo (n = 6 per group per time point) by a certified veterinary pathologist (Charles River Laboratories, Wilmington, MA) who was blinded to the treatment groups. Indices of pathology were scored as 0–5: 0 = normal, 1 = minimal/slight response, 2 = mild response, 3 = moderate response, 4 = marked response, and 5 = severe response.

The enhanced darkfield microscopy (EDM) makes use of high signal-to-noise illumination and allows to visualize nanoparticles in cells and tissues with strong light scattering properties (Hubbs et al., 2013; Mercer et al., 2013b). This imaging technique was used to visualize uptake of BNNT particles by macrophages over time. Briefly, 10^5 BAL cells from each mouse were spun down onto slides with a Cytospin 3 centrifuge (Shandon Life Sciences International, Cheshire, England) and were viewed by a Cyto-Viva EDM (CytoViva, Auburn, AL). The lung tissue sections were prepared using laser cut slides and coverslips (Schott North America, Inc., Elmsford, NY) to avoid contamination of silica particles. The sections were also viewed under the same EDM. Images were analyzed with a CytoViva plugin to ENVI 4.0 Software licensed to and distributed by CytoViva Inc. (CytoViva Inc., Auburn, AL, USA).

Pulmonary clearance was evaluated in a third set of mice aspirated with 40 μg of BNNT or DM by measuring lung burden of boron at 1 d, 7 d, 1 mo, and 2 mo post-exposure (n = 5 per time point) by inductively-coupled plasma-atomic emission spectroscopy (ICP-AES). Lung digestion and measurements followed the EPA Method 6010B (ALS Global, Cincinnati, OH) (EPA, 1996). The standard was prepared following EPA Method 6010B Section 5.3.6 with reagent grade boron. In this method the tissue digestion was performed in plastic vessels to avoid boron contamination from glassware. The limit of detection varied by batch from 0.6 to 1.1 mg/kg. It is important to note that this measure is for boron and not specific for the various forms of boron in the BNNT sample.

2.7. RNA isolation and gene expression

RNA was isolated from frozen lung and liver (n = 8 per group per time point) using the RNeasy Mini Kit (Qiagen, Valencia CA) following homogenization using a Tissue Lyser II (Qiagen, Valencia, CA). A 2 ul aliquot of each RNA sample was quantified using a NanoDrop One spectrophotometer (Thermo Fisher Scientific, Madison WI). Evaluation of gene expression was determined by standard 96-well technology using the StepOne™ (Applied Biosystems, Carlsbad, CA, USA) with predesigned Assays-on-Demand™ TaqMan® probes and primers. Assessed genes for the lung included Interleukin-6 (*Il6*, Mm00446190_m1), macrophage inflammatory protein (MIP)-2 (*Ccl2*, Mm00441242_m1), monocyte chemotactic protein (MCP)-1 (*Cxcl2*, Mm00436450_m1), macrophage-derived chemokine (MDC) (*Ccl22*, Mm00436439_m1), osteopontin (*Spp1*, Mm00436767_m1), IL-1beta (*Il1β*, Mm01336189_m1), IL-5 (*Il5*, Mm00439646_m1), and eotaxin (*Ccl11*, Mm00441238_m1); for the liver included serum amyloid P-component (*Apcs*, Mm00488099_g1), metallothionein 1 (*Mt1*, Mm00496660_g1), metallothionein 2 (*Mt2*, Mm00809556_s1), serum amyloid A1 (*Saa1*, Mm00656927_g1), and haptoglobin (*Hp*, Mm00516884_m1). Using 96 well plates, 1 μg of total RNA was reverse transcribed using random hexamers (Applied Biosystems) and Superscript III (Invitrogen, Carlsbad, CA). Nine microliters of cDNA (5 ng/μl) was then used for gene expression determination. Hypoxanthine-guanine phosphoribosyl transferase (*Hprt*) was used as a housekeeping gene. Relative gene expression was calculated using the comparative threshold method ($2^{-\Delta\Delta Ct}$) with vehicle-treated mice serving as the reference group (Schmittgen and Livak, 2008).

2.8. Statistics

For histopathological data, which are inherently categorical, a nonparametric analysis of variance was performed using Wilcoxon rank sum test by SAS/STAT software (SAS Institute, Inc., Cary, NC). All other data were analyzed using SAS version 9.4 for Windows using two-way analyses of variance with treatment and time as the main factors and the interaction included. *Post hoc* comparisons were carried out using Fishers LSD. All variables with the exception of the white blood cell data were transformed with the natural log prior to the analysis to correct for heterogeneous variance. Data points that fell below the limit

of detection in the cytokine analysis were assigned the value of half the limit of detection for the given cytokine prior to log transformation. Criterion for significance was set at $p < 0.05$ for all data. Criterion for significance was set at $p < 0.05$ for all data. Results are presented as mean ± standard error. Significant difference between group within a time point are indicated in the figures and table. Additionally, significant differences across time within a group are described in the Results section.

3. Results

3.1. Particle characterization

FESEM was employed to visualize the lateral dimension of the primary particle size of the BNNT sample in dry powder form (Fig. 1). The "as-produced" form prior to dispersion is shown in Fig. 1A. These samples were manufactured to have dimensions of 5 nm wide and up to 200 μm long and are collected in a "puffball" form. The as-produced sample is ~50% BNNT covalently bound to primarily hBN. Fig. 1B–E show FESEM images of the dispersed BNNT sample at various stages in the process of preparation for *in vivo* administration: in ethanol (B), followed by drying and dispersion in DM (C, low magnification; D and E, high magnification). Fig. 1F is a transmission electron micrograph (TEM) of BNNT collected on a personal air sample filter at the facility during manufacturing operations illustrating the similarities between the dispersion for *in vivo* studies *versus* and the agglomeration state of the material in the breathing zone of a worker, where respirable air concentrations ranged from 0.01–0.03 mg/m^3 (0.01–0.03 μg/l) over ~8 h per day prior to additional placement of engineering controls (NIOSH, 2017, company communication).

The sonication and preparation process significantly disrupted BNNT length. The sonication process also may result in the release of a degree of free hBN from the tube structures as well. In DM, following sonication preparation for *in vivo* exposures, BNNT agglomerates were loose in structure and ranged in size up to 20 μm in diameter (Fig. 1C). The dispersed BNNT were measured to have a diameter of approximately 13–23 nm, and length on average of ~0.6–1.6 μm. DLS was used to measure agglomerate size distribution in DM for the BNNT sample, which resulted in a hydrodynamic diameter of 773.0 ± 22.4 nm ($n = 10$). Although the nature of the agglomeration was structurally similar to that on the personal breathing zone filter, the agglomerate size following dispersion was smaller whereby agglomerate sizes on the filter were primarily in the 2–5 μm size range (NIOSH, 2017,company communication). Specific surface area (SSA) was measured by the BET method using gas adsorption and found to be 182.6 ± 2.4 m^2/g. The density of the as-produced BNNT sample was measured to be 0.03 g/cm^3. Both of SSA and density were comparable to that reported by the manufacturer, ~200 m^2/g and 0.025 g/cm^3, respectively. Zeta potential of the sample in DM at pH 7.4 was measured as −18.0 ± 0.80 mV ($n = 5$), indicative of negative charge and moderate instability of the agglomerates of BNNT in DM. Electron paramagnetic resonance spectroscopy indicative of surface reactivity of the material in DM is shown in Fig. 2. The spin trap, DMPO, did not produce a signal indicative of its purity. The DM control also did not produce a free radical signal in the presence of H_2O_2. BNNT did produce a signal in the presence of H_2O_2; however, the signal was relatively low compared to that of the positive control, copper nanoparticles, indicative low levels of free radicals associated with the surface of the material.

3.2. In vivo toxicity

3.2.1. Dose relevance

The deposition fraction was calculated using the Multiple-Path Particle Dosimetry MPPD software v3.04 (Applied Research Associates, Inc., Albuquerque, NM). Default values were used for settings with the exception of the following which were applied based on particle characterization analyses: Human Yeh/Schum Symmetric was applied for airway morphometry; density of 0.03 g/cm^3, equivalent diameter for agglomerates of 0.773 μm CMD, and inhalability adjustment of GSD 1.1 based on DLS measures of agglomerate size were applied for inhalant properties; breathing frequency of 17.5 min^{-1}, tidal volume 1143 ml, and oronasal mouth were applied for exposure conditions; and deposition only was selected for deposition/clearance calculation as the mouse model was a single bolus dose. The total deposition fraction was 0.0976 with 0.0120 in the head region, 0.0403 in the tracheobronchial region, and 0.0453 in the alveolar region. Given the route of administration to mice and the parameters examined, the alveolar region value was selected for calculating the human dose equivalent. Lung

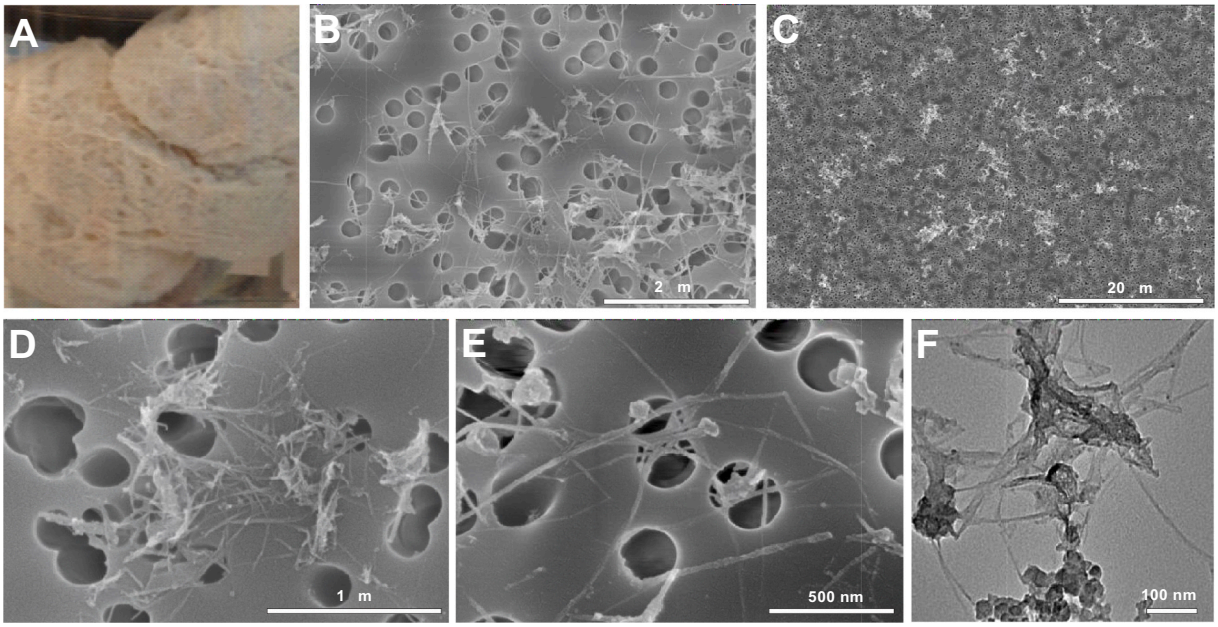

Fig. 1. BNNT sample in bulk "as-produced" form prior to dispersion (A). FESEM images of dispersed BNNT in ethanol (B) followed by drying and dispersion in DM (C, low magnification; D, E high magnification). TEM image BNNT collected on a filter from a personal air sample at the facility (F).

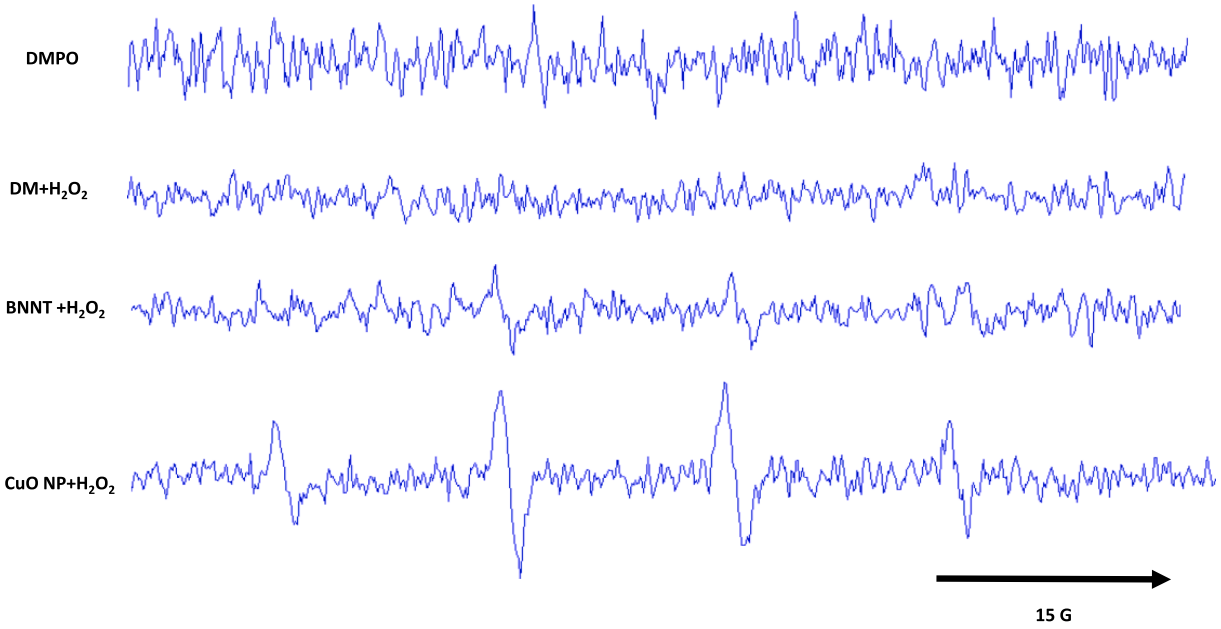

Fig. 2. Electron paramagnetic resonance spectra as a measure for surface reactivity for DMPO alone, DM + H_2O_2, the high dose concentration of BNNT + H_2O_2, and the positive control, copper nanoparticles, at the same concentration + H_2O_2.

deposition for a worker is shown in EQ1:

$$\text{EQ1} = (\text{field concentration}, \mu g/l) \times (\text{minute ventilation}, l/\text{min}) \times (\text{exposure time per d}, \text{min/d}) \times (\text{alveolar deposition efficacy, unitless})$$

Respirable air concentrations of total particulate at the facility ranged from non-detectable (below the detection limit of 0.01 mg/m^3) up to 0.036 mg/m^3 in the personal breathing zone of the worker, depending on the location of sampling in the facility. Where detectable, levels were highest in growth/harvesting/cleaning and production application areas; however, it is important to note that these levels were in the lower range of equipment detection. For the purpose of this estimation, we have assumed that the total particulate was comprised primarily of the BNNT sample. Using a lower and higher measurement from the field study of 0.01 mg/m^3 (0.01 μg/l) and 0.03 mg/m^3 (0.03 μg/l), assuming moderate work (~31% sitting, ~68.8% standing) for a minute ventilation of 20 L/min and an 8 h workday (480 min) (ICRP, 1994), an alveolar deposition fraction of 0.0453, and assuming no pulmonary clearance, the daily deposited dose was calculated to be 4.35 μg at 0.01 mg/m^3 and 13.0 μg at 0.03 mg/m^3. Normalizing the deposited doses of 4.35 and 13.0 μg per day in the human lung with alveolar surface area of 102.2 m^2 to the surface area of a mouse lung of 0.05 m^2 (Stone et al., 1992), the equivalent deposited dose in the mouse was 0.0021 and 0.0064 μg/d. Therefore, the doses of 4 and 40 μg represent between 625–1,905 days and 6250–19,050 days, respectively. Adjusting the number of days for a work year of 260 d/year, the doses represent ~2.4–7.3 years for the 4 μg low dose and ~24.0–73.3 years for the 40 μg high dose.

3.2.2. BAL fluid analysis

As an index of cytotoxicity and lung injury, lactate dehydrogenase (LDH) activity was analyzed in the BAL fluid collected from mice at 4 h, 1 d, 7 d, 1 mo, and 2 mo post-exposure to BNNT (Fig. 3). Exposure to the high dose BNNT significantly increased LDH at earlier time points from 4 h to 7 d post-exposure when compared to the low dose and control groups at all time points and compared to the BNNT high dose group at 1 and 2 mo post-exposure. Although injury was still significantly increased at 1 mo post-exposure, LDH activity levels decreased after 7 d, and had returned to control levels by 2 mo, indicating resolution of lung injury over time. The low dose of BNNT did not cause lung injury indicated by LDH activity at any time point.

A panel of 32 proteins in BAL fluid was measured reflecting the activity of cellular pathways including chemotaxis, inflammation, and immune response. Fig. 4 is a heat map representing all the cytokines measured. The cytokine/chemokines from BAL fluid of mice exposed to BNNT is presented as log 2-fold change from cytokine/chemokines of DM exposed mice. The high dose of BNNT caused increased proteins related to inflammation and immune cell activation, with the most persistent response related to recruitment of macrophages and neutrophils to the lung (KC, G-CSF, MIP-2and MIP-1α), irritant response (IL-5, Eotaxin), and IP-10 which is involved in both monocyte and immune cell recruitment. Protein levels changed significantly in both dose- and time-dependent manners, whereby the majority of proteins returned to control levels by 2 mo with the exception of KC and IP-10 KC was significantly greater at the 1 d timepoints when compared to all other timers within the high dose group, and both KC and IP-10 were

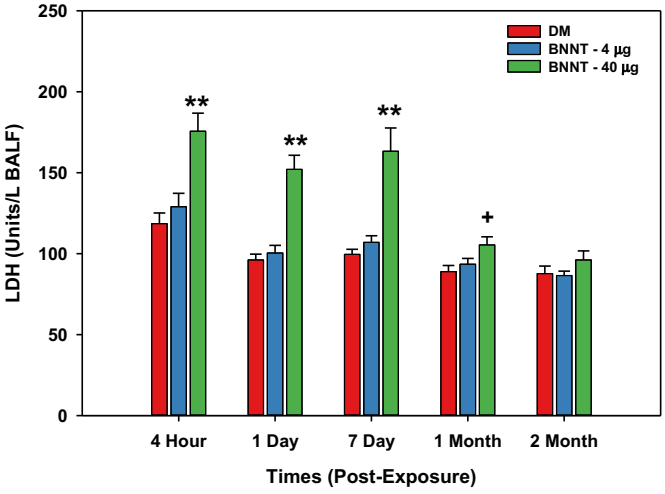

Fig. 3. Lactate dehydrogenase (LDH) activity, an indicator of cytotoxicity, BAL fluid recovered from mice 4 h, 1 d, 7 d, 1 mo, and 2 mo post-exposure to 4 or 40 μg of BNNT, or DM alone (n = 8 per group per time point). **Significantly different from all groups within a time point, $p < 0.01$; +significantly different from DM within a time point, $p < 0.05$.

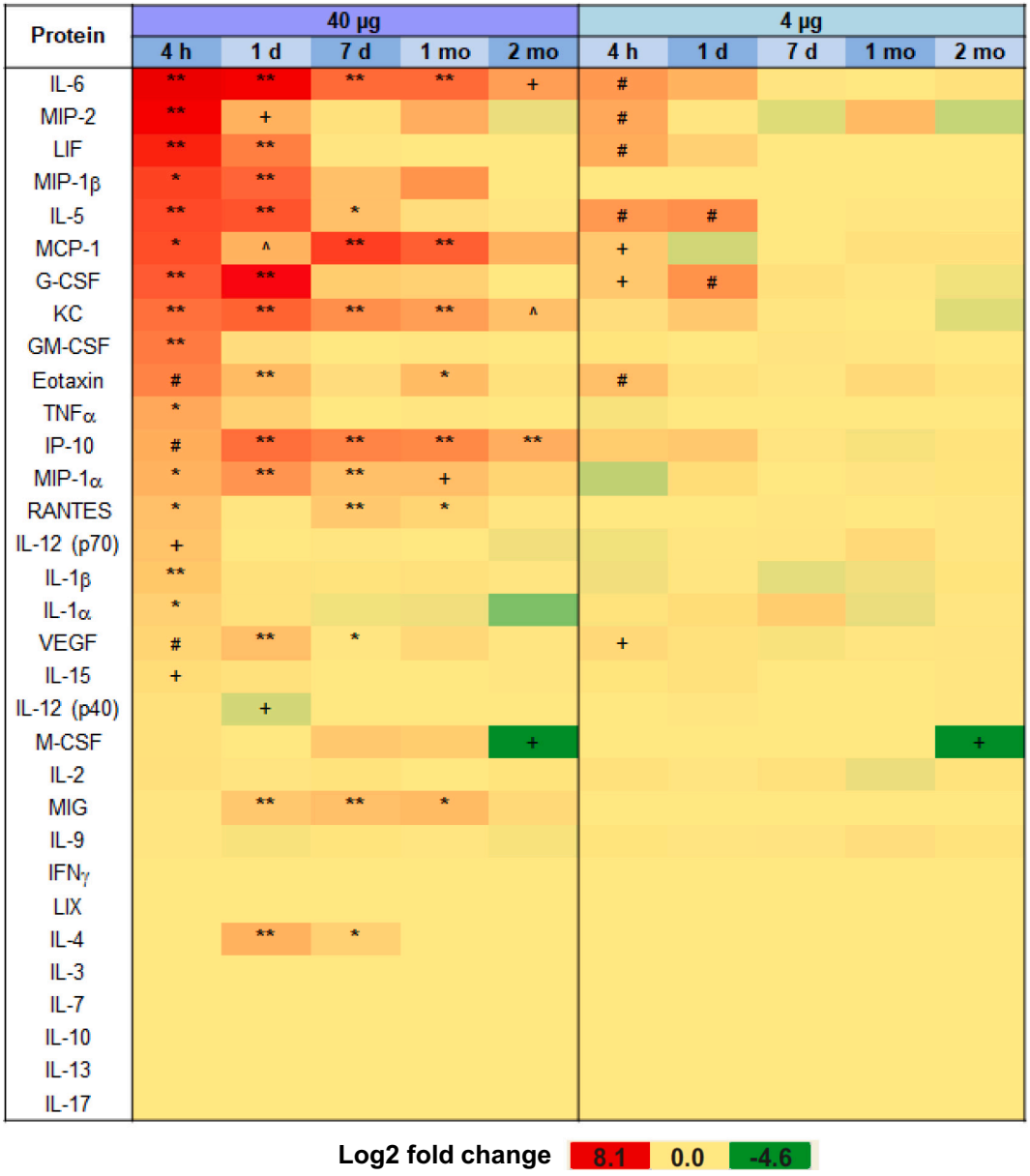

Fig. 4. Heat map of proteins from a 32-plex analysis panel that were significantly increased in BAL fluid recovered from mice at 4 h, 1 d, 7 d, 1 mo, and 2 mo post-exposure to 4 or 40 µg of BNNT, or DM alone ($n = 6$ per group per time point). Data presented as fold change *versus* DM control, with yellow through red as increasing values and yellow through green as decreasing values. **Significantly different from all groups within a time point, $p < 0.01$; *significantly different from all groups within a time point, $p < 0.05$; #significantly different from DM within a time point, $p < 0.01$; +significantly different from DM within a time point, $p < 0.05$; ^significantly different from BNNT low, $p < 0.05$.

significantly lower at the 2 mo time point within the group showing a trend for resolution as well. Cytokines involved in immune cell activation including IL-4 and RANTES were also significantly increased resolving by 1 mo and 2 mo, respectively. There was also a significant increase in several proteins in the low dose group at the early time points when compared to control. These included MIP-2, MCP-1, LIF, G-CSF, IL-5, IL-6, Eotaxin, and VEGF. The resolution of response occurred more rapidly than in the high dose group. Within the low dose group, IP-10 and KC also showed significant time-dependent changes; however, these proteins were not elevated significantly when compared to controls at a given time point. The following proteins were not significantly altered in either group: IFNγ, IL-2, IL-3, IL-7, IL-9, IL-10, IL-13, IL-17, LIX.

3.2.3. BAL cell profile

Cell counts and differentials were performed on cells recovered by BAL at 4 h, 1 d, 7 d, 1 mo and 2 mo post-exposure (Fig. 5). Exposure to the high dose of BNNT caused an increase in inflammation, indicated by significantly increased macrophage (Fig. 5A) and neutrophil influx into the lungs (Fig. 5B), as well as an irritant response, indicated by significantly increased eosinophils (Fig. 5C). Macrophages increased significantly compared to all groups at 7d. Within the high dose group, macrophages were significantly increased at 7 d compared with 4 h, 1 d and 2 mo, and the 1 and 2 mo levels of macrophages were significantly elevated when compared to 4 h. The high dose of BNNT caused a significant increase in neutrophils compared to all groups at 4 h, 1 d, and 7

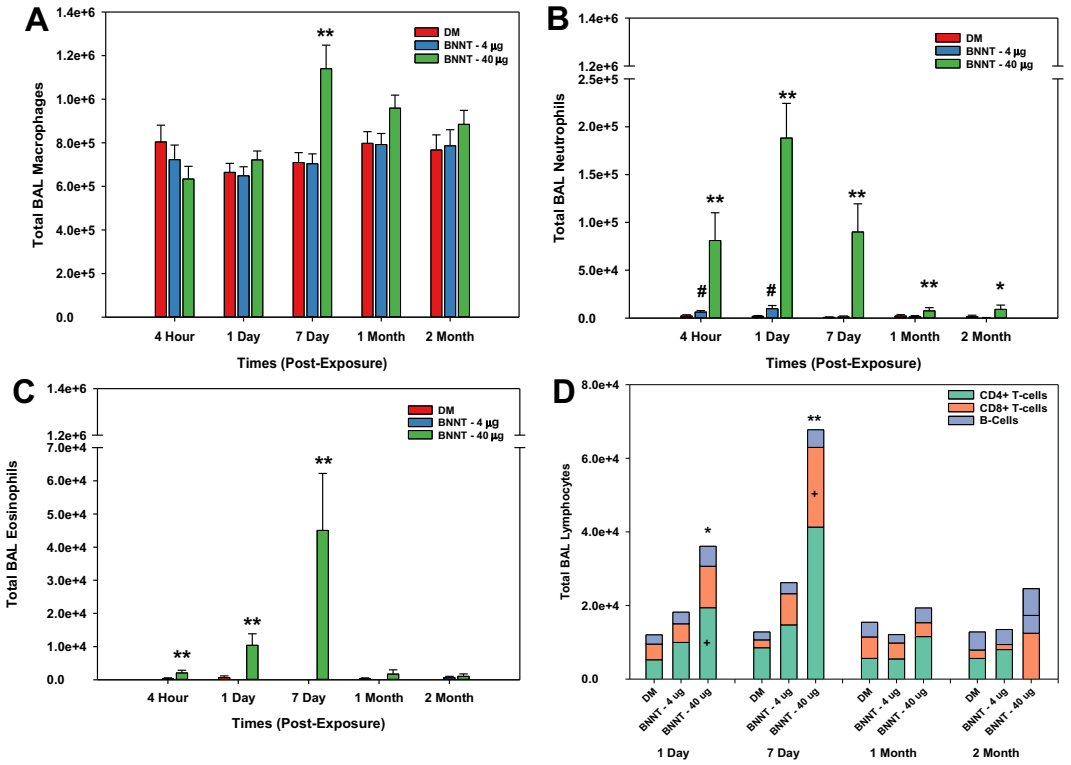

Fig. 5. Macrophages (A), neutrophils (B), and eosinophils (C) recovered by BAL from mice 4 h, 1 d, 7 d, 1 mo, and 2 mo following exposure to 4 or 40 µg of BNNT or DM alone(n = 8 per group per time point). (D) Total lymphocytes and phenotype, enumerated by flow cytometry recovered by BAL from mice 1 d, 7 d, 1 mo, and 2 mo following exposure to 4 or 40 µg of BNNT or DM alone. Symbols above the bar in panel D refer to significant changes to the total number of lymphocytes and symbols within the bars refer to significant changes in the subpopulations. ** Significantly different from all groups within a time point, $p < 0.01$; *significantly different from all groups within a time point, $p < 0.05$; #significantly different from DM within a time point, $p < 0.01$.

d, with a peak at 1 d. The increase at these time points was significant compared to 1 and 2 mo showing a significant degree of resolution over time. The low dose also caused a significant increase at 4 h and 1 d compared to DM and to low dose levels at 7 d, 1 mo, and 2 mo indicative of resolution over time. Eosinophils increased significantly at the early time points in the high dose group compared to all other groups. This increase peaked at 7 d where the response was significantly greater than at 4 h, 1 mo, and 2 mo.

BAL lymphocytes were phenotyped by flow cytometry. In addition to phagocytic influx described in Fig. 5A–C, exposure to high dose of BNNT caused significantly increased lymphocyte influx into the lung at 1 d and 7 d post-exposure when compared to all other groups (Fig. 5D). The increase was primarily due to CD4+ and CD8+ T cell population subsets (green and orange, respectively). The influx in the high dose group was significantly lower at 1 and 2 mo post-exposure indicating a degree of resolution in response. There was no significant difference between low dose BNNT and DM control groups.

3.2.4. *Lung histopathology, phagocytosis, and pulmonary clearance*

Histopathological analysis for hyperplasia, hypertrophy, development of lymphoid tissue, alveolar thickening, and mixed leukocyte infiltration (ML) in the perivascular/peribronchiolar (PV/PB) region, the

Table 1
Histopathology analysis of lung tissue following exposure to BNNT particles.

Time (post-exposure)	Treatment group	ML – PV/PB	ML - AS	ML -AL	ML - BL
1 D	DM	0.17 (1/6)	0.17 (1/6)	0.17 (1/6)	–
	BNNT-4 µg	–	–	0.17 (1/6)	–
	BNNT-40 µg	0.17 (1/6)	–	0.83 (5/6)*	0.17 (1/6)
7 D	DM	–	–	–	–
	BNNT-4 µg	–	–	–	–
	BNNT-40 µg	1.00(6/6)*	0.50 (3/6)	1.17 (6/6)*	–
1 Mo	DM	–	–	–	–
	BNNT-4 µg	–	–	–	–
	BNNT-40 µg	–	–	0.83 (5/6)*	–
2 Mo	DM	–	–	–	–
	BNNT-4 µg	–	–	0.17 (1/6)	–
	BNNT-40 µg	–	–	0.50 (3/6)	0.17 (1/6)

Note: Lung tissue was analyzed for hyperplasia, hypertrophy, development of lymphoid tissue, alveolar thickening, and mixed leukocyte infiltration (ML) in the perivascular/peribronchiolar (PV/PB) region, the alveolar septae (AS), alveolar lumen (AL), and bronchiolar lumen (BL) (n = 6 per group per time point). Severity was scored as 0–5: 0 = normal, 1 = minimal/slight, 2 = mild, 3 = moderate, 4 = marked, and 5 = severe. Data are presented as means with incidence (number of animals with a positive score per total animals) in parentheses. Significant findings are labeled with *, $p < 0.05$. No changes in type II cell hyperplasia, hypertrophy, lymphoid tissue, or septal thickening were noted.

alveolar septae (AS), alveolar lumen (AL), and bronchiolar lumen (BL) was performed at 1 d, 7 d, 1 mo, and 2 mo post-exposure for both low dose and high dose groups ($n = 6$ per group per time point) (Table 1). No alveolar septal thickening, hypertrophy, or hyperplasia were present in any groups. The only finding of significance was a minimal level of inflammatory cell infiltration (neutrophils and macrophages) in the high dose BNNT group, which was greatest at 7 d and diminished at 2 mo post-exposure.

BNNT in lung tissue was visualized by EDM (Fig. 6A). At the early time point of 1 d post-exposure, some BNNT particles can be observed along the lining on the alveola septae in the high dose group (Green arrows in Fig. 6A); however, the majority of the BNNT particles are located in the macrophages in focal areas of inflammation. Areas of condensed tissue with macrophages that have phagocytized BNNT particles were observed primarily at 7 d post-exposure. By the end of the study, at 2 mo post-exposure, BNNT are still observed within macrophages; however, focal areas of inflammation were mostly resolved compared to 7 d. The uptake of BNNT particles by alveolar macrophages in BAL was also visiualized by the EDM (Fig. 6B). Macrophage phagocytosis appeared dose-dependent. Particle uptake by macrophages continued throughout the time course of the study but was noted to be highest at 7 d, which is in agreement with the histopathology analysis.

The lung burden of boron following the high dose of BNNT (40 μg per mouse) in the whole lung was measured at 1 d, 7 d, 1 mo, and 2 mo post-exposure by ICP-AES. Data from the measurements was presented as percent of the boron burden at 1 d (Fig. 7). The error in measurement at the early time points was high; however, by 1 mo post-exposure, the lung burden was decreased to ~47%. Overall, the data indicated there was ~50% clearance of boron in the lung from early time point to the end of the study. It should be noted that the assumption here is that the boron measurement is representing the whole BNNT sample. Although the non-nanotube fraction of the sample is covalently bound to the BNNT, the different forms of boron may undergo different rates of dissolution in the sample and therefore be cleared from the lungs at different rates and potentially overestimating the rate of clearance of the BNNT fraction of the sample.

3.2.5. Relative mRNA expression in lung

A panel of eight genes related to inflammation, irritant response, and immune response, including *Cxcl2*, *Ccl22*, *Il6*, *Ccl2*, *Spp1*, *Il1b*, *Il5*, and *Ccl11*, were analyzed in the lungs. At 4 h post-exposure, seven out of eight genes, with the exception of *Spp1*, were significantly elevated for both low dose and high dose BNNT groups in a dose-dependent manner (Fig. 8), indicating acute inflammation in the lung. For all of these genes, there was a significant reduction in expression by 1 d; however, in the high dose group, despite the reduction following the 4 h time point, *Cxcl2*, *Ccl22*, *Il6*, *Ccl2* remained significantly elevated when compared to all groups and this persisted equivocally up to 2 mo. These genes encode for MIP-2, MDC, IL-6, and MCP-1, respectively, indicating a degree of persistent inflammation in the lung following the high dose over time. *Il1b* gene expression, encoding for IL-1β expression which is associated with inflammasome formation, had returned to control levels in the high dose group by 1 mo. In the high dose group, *Il5* and *Ccl11*, genes encoding for IL-5 and eotaxin, returned to control levels by 1 d, but this was followed by a significant increase 7 d and 1

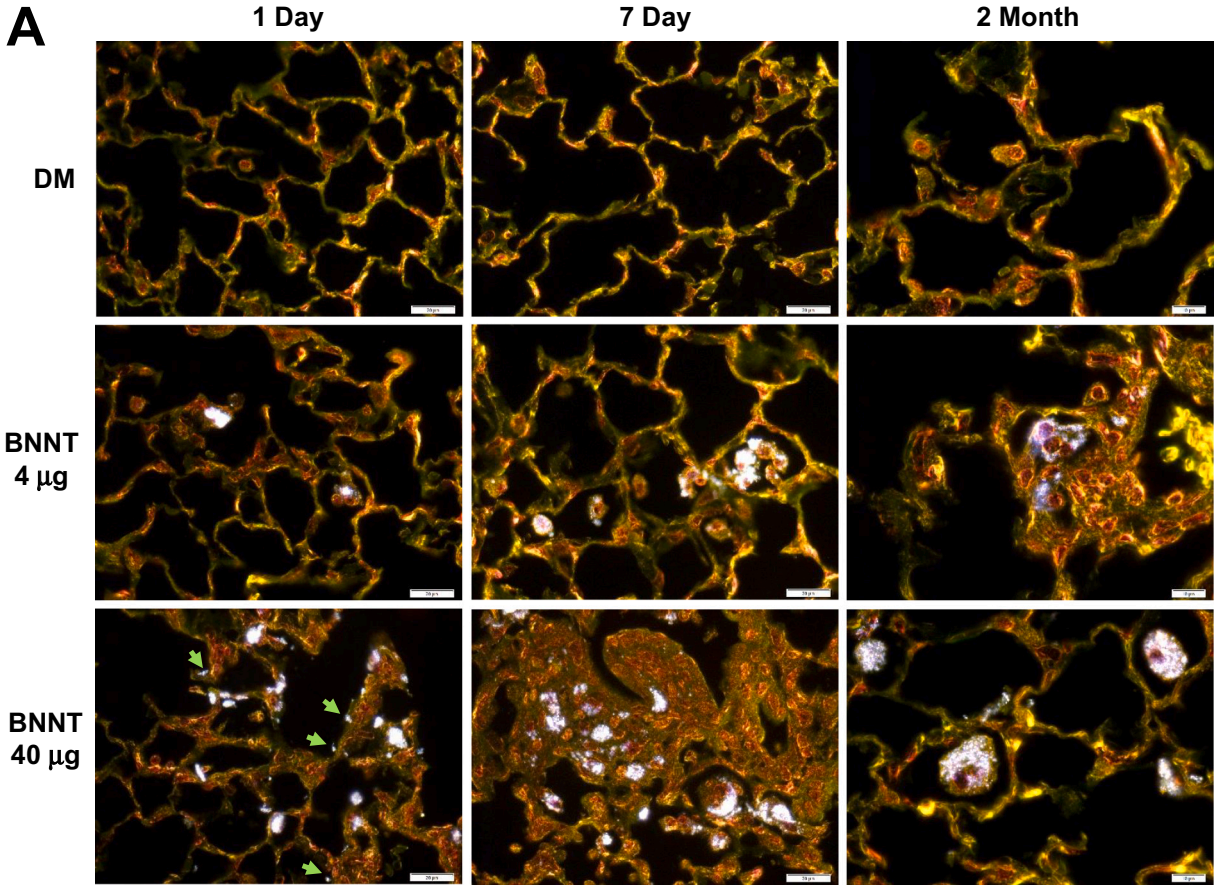

Fig. 6. Enhanced darkfield images. (A) Lung tissue slides from mice at 1 d, 7 d, and 2 mo post-exposure to 4 or 40 μg of BNNT or DM alone. (B) Cytospins of cells recovered by BAL from mice at 1 d, 7 d, and 2 mo following exposure to 4 or 40 μg of BNNT or DM alone. BNNT appear as bright white or blue within macrophages. Cell nuclei in these micrographs are red to brown. The green arrows indicate the particles along the lining on the alveola septae. Calibration marker is 20 μm for 1 d and 7 d, and 10 μm for 2 mo.

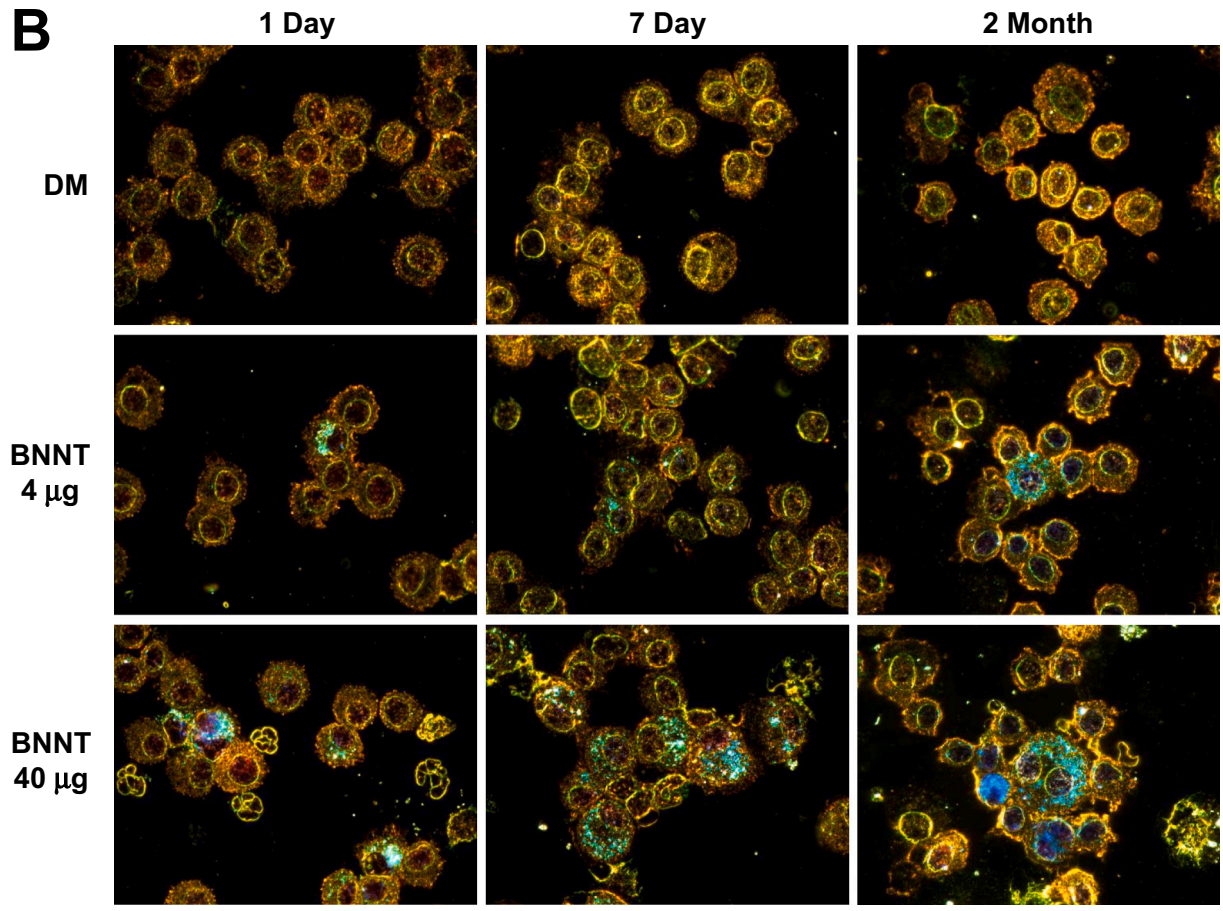

Fig. 6. (*continued*)

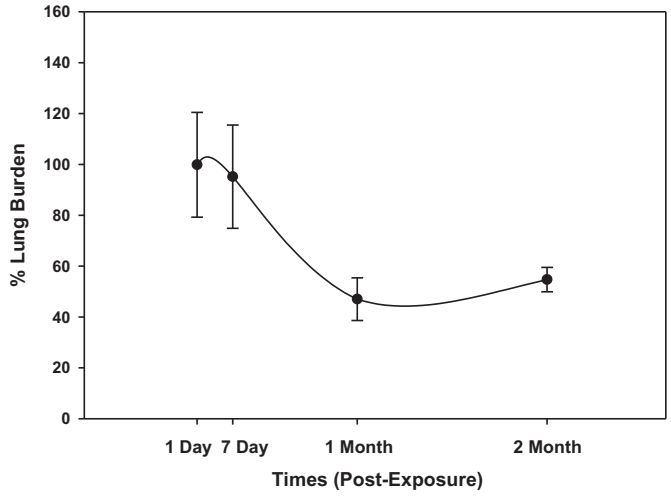

Fig. 7. Lung burden from mice at 1 d, 7 d, 1 mo, and 2 mo post-exposure to 40 µg of BNNT presented as percent of boron in the lungs on 1 d (n = 5 per group per time point).

mo corresponding to an increase in lung eosinophils at 7d. The response resolved significantly by 2 mo. *Spp1*, which can be suggestive of granuloma production and immune responses, as well as injury and repair tissue repair process, was significantly increased by the high dose of BNNT from 1 d to 2 mo post-exposure, and peaked at 7 d post-exposure. *Il5* and *Ccl11*, indicators of irritant response, were highly induced at 4 h post-exposure of BNNT, with resolution at later time points. The low dose of BNNT exposure only increased gene expression at 4 h post-exposure, with no effect at time points after 1 d post-exposure.

3.2.6. Lung MLN and spleen lymphocyte profile

MLN and spleen lymphocytes were also phenotyped by flow cytometry. All MLN lymphocytes measured (CD4+ T-cells, CD8+ T-cells, and B cells), as well as natural killer (NK) cells were significantly increased in the high dose BNNT group at 7 d post-exposure when compared to all other groups (Fig. 9A). The increase in B cells at 7 d in the high dose groups was significant compared to 1 d and 2 mo in the same group. The increase in CD4+ and CD8+ T-cells at 7 d was significant when compared to all other time points indicating resolution of the response over time. There was a small but significant increase in total lymphocytes in MLN in the low dose group at 4 h; however, the increases in the subsets were not significant. Similar analysis was performed on spleen lymphocytes at both doses. No significant differences were observed in any group at any time point (data not shown).

3.2.7. White blood cell profile

White blood cells (WBC) were counted and differentiated (PMN, lymphocytes, monocytes, and eosinophils) to evaluate the systemic response (Fig. 9B). The changes in WBC showed no consistent pattern over time. There was an overall decrease in circulating WBC in the high dose group at 4 h and this was due primarily to the lymphocyte population. At 1 mo post-exposure in the high dose group there was a significant increase basophil number. At 2 mo, there was a significant increase in total circulating WBC in the high dose group compared to all groups and the high dose group at all time points. This increase was due primarily to a significant increase in the lymphocyte population. In the low dose group, neutrophils were significantly lower than control and

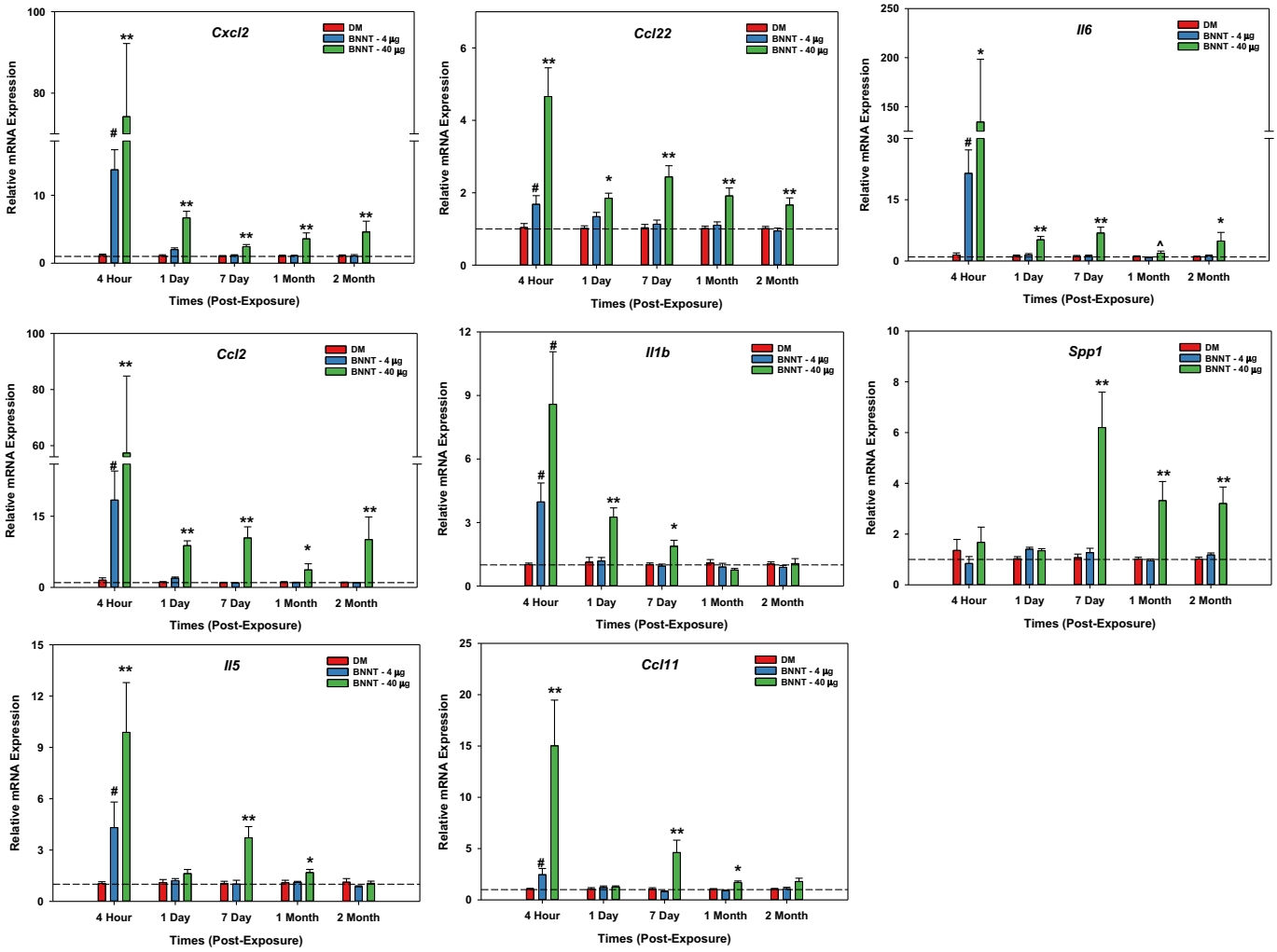

Fig. 8. Gene expression in lung tissue. Relative mRNA expression of MIP-2 (*Cxcl2*), MDC (*Ccl22*), IL-6 (*Il6*), MCP-1 (*Ccl2*), osteopontin (*Spp1*), IL-1b (*Il1b*), IL-5 (*Il5*), and eotaxin (*Ccl11*) relative to DM control at all time points post-exposure (n = 8 per group per time point). **Significantly different from all groups, $p < 0.01$; *significantly different from all groups, $p < 0.05$; #significantly different from DM, $p < 0.01$; +significantly different from DM, $p < 0.05$; ^significantly different from BNNT low, $p < 0.05$.

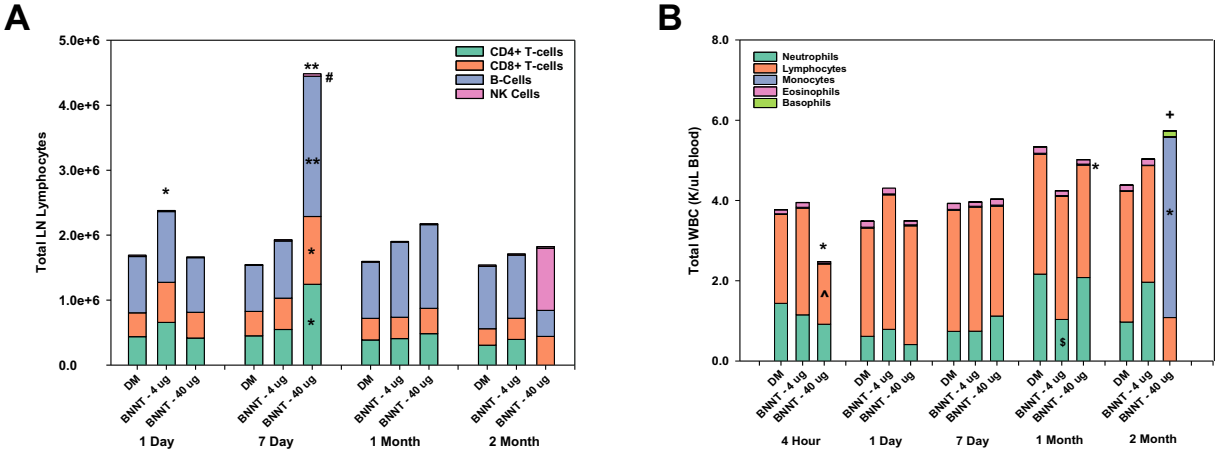

Fig. 9. Systemic cellular responses in mice 1 d, 7 d, 1 mo, and 2 mo following exposure to 4 or 40 µg of BNNT or DM alone (n = 8 per group per time point). Total lung-associated lymph node (LN: mediastinal) lymphocytes and phenotype, enumerated by flow cytometry recovered by BAL (A) and total White blood cell (WBC) counts and phenotype (B). Symbols above the bar in panel A and B refer to significant changes to the total number of cells and symbols within the bars refer to significant changes in the subpopulations. The hashtag to the right of the BNNT 40 µg group at 7 d in panel A due indicates a significant increase in NK cells compared to DM. The asterisk to the right of the BNNT 40 µg group indicates significance for basophil population. **Different from all groups, $p < 0.01$; *significantly different from all groups, $p < 0.05$; +significantly different from DM, $p < 0.05$; ^significantly different from BNNT low, $p < 0.05$; $significantly different from DM and BNNT 40 µg group, $p < 0.05$.

high dose at 1 mo. There were no other significant differences in monocyte, lymphocyte, neutrophil, basophils, or eosinophil number between the low dose group and control group at any other time point.

3.2.8. Relative mRNA expression in liver

Liver acute phase response and oxidative stress genes, *Mt1*, *Mt2*, *Saa1*, *Apcs*, and *Hp*, were measured in the liver tissue (Fig. 10). Expressions of *Mt1* and *Mt2* were significantly elevated by high dose BNNT at 4 h post-exposure compared to all groups at all time points post-exposure. High dose of BNNT also increased *Saa1* gene expression at 4 h and 1 d post-exposure when compared to all groups, but this elevation was significantly resolved by 7 d post-exposure. *Apcs* and *Hp* gene expression were only increased by the high dose of BNNT at 1 d post-exposure when compared to all groups at all times. There were no significant differences between low dose BNNT and DM gene expression.

4. Discussion

There is currently very limited information available on *in vivo* toxicity of BNNT, particularly pulmonary toxicity. To date, the current study is the first *in vivo* study to investigate the time course of BNNT toxicity in the lung. The as-produced BNNT sample used in this study was a complex particle containing ~50–60% BNNT with the remaining portion of the sample composed of covalently bound hBN, as well as boron and amorphous boron nitride as a result of the synthesis process (Smith et al., 2009). The size of the primary BNNT in the as-produced BNNT samples was targeted to be 5 nm in diameter and up to 200 μm in length. After the sonication and preparation process for *in vivo* studies which disrupts the length in the process, the size of BNNT samples was shown to have the diameter of approximately 13–23 nm, and length on average of ~0.6–1.6 μm. Although the preparation process changed the dimension of the sample, the dispersion in DM was very similar to samples that were collected from the personal breathing zone of workers at the facility (Fig. 1F). The results from the current study showed that the high dose of this BNNT sample (40 μg per mouse), which was estimated to be equivalent to ~2–7 decades of work exposure in a single dose, caused the greatest degree of injury and inflammation in the lungs at early time points, 4 h, 1 d, and 7 d, post-exposure. This injury was indicated by increased LDH activity, BAL granulocyte infiltration into the lung, increased cytokines and chemokines associated with inflammation and immune response, and alterations in lung gene expression related to inflammation. The majority of these effects resolved by 2 mo post-exposure and did not cause fibrosis or bronchiolitis obliterans, as has been observed in similar dose and time-course mouse models following exposure to MWCNT (Bishop et al., 2017; Porter et al., 2010). The low dose used in this study (4 μg per mouse), estimated to be equivalent to ~2–7 years of exposure in a single dose, caused little to no toxicity.

There are very few BNNT *in vivo* studies with which to compare the findings of the current study. Results from previous *in vivo* studies of BNNT were also contradictory (Ciofani et al., 2012, 2013; Kodali et al., 2017; Salvetti et al., 2015), with only one acute pulmonary toxicity study that reported inflammation *in vivo* 24 h post-exposure to the same commercial grade BNNT sample used in the current study (Kodali et al., 2017), which is in agreement with the study here. Contrarily, studies from Ciofani et al. and Salvetti et al. (Ciofani et al., 2012, 2013; Salvetti et al., 2015) showed no toxicity induced by BNNT *in vivo*. Ciofani et al. injected rabbits intravenously with 1 mg/kg BNNT (Ciofani et al., 2012) or up to 10 mg/kg BNNT (Ciofani et al., 2013) and the blood test results after 3 d or 7 d showed no impairments in blood, liver and kidney functionality. Salvetti et al. (2015) investigated the effects of BNNT in freshwater planarians. They conducted a short-term acute effect study by a single injection of 100 or 200 μg/g BNNT and a long-term effect (subchronic) by injection twice a week for 15 d to receive a total amount of 100 or 200 μg/g BNNT. The results from their studies showed no induction of oxidative DNA damage and apoptosis and no adverse effects on planarian stem cell biology. Comparisons with the current study are complicated by differences in species, route of exposure, delivered dose, and physicochemical differences in the BNNT samples.

As BNNT is a structural analog of MWCNT, the present study was designed to be comparable to previous MWCNT studies conducted by our collaborators and other investigators in both dose (4 or 40 μg of

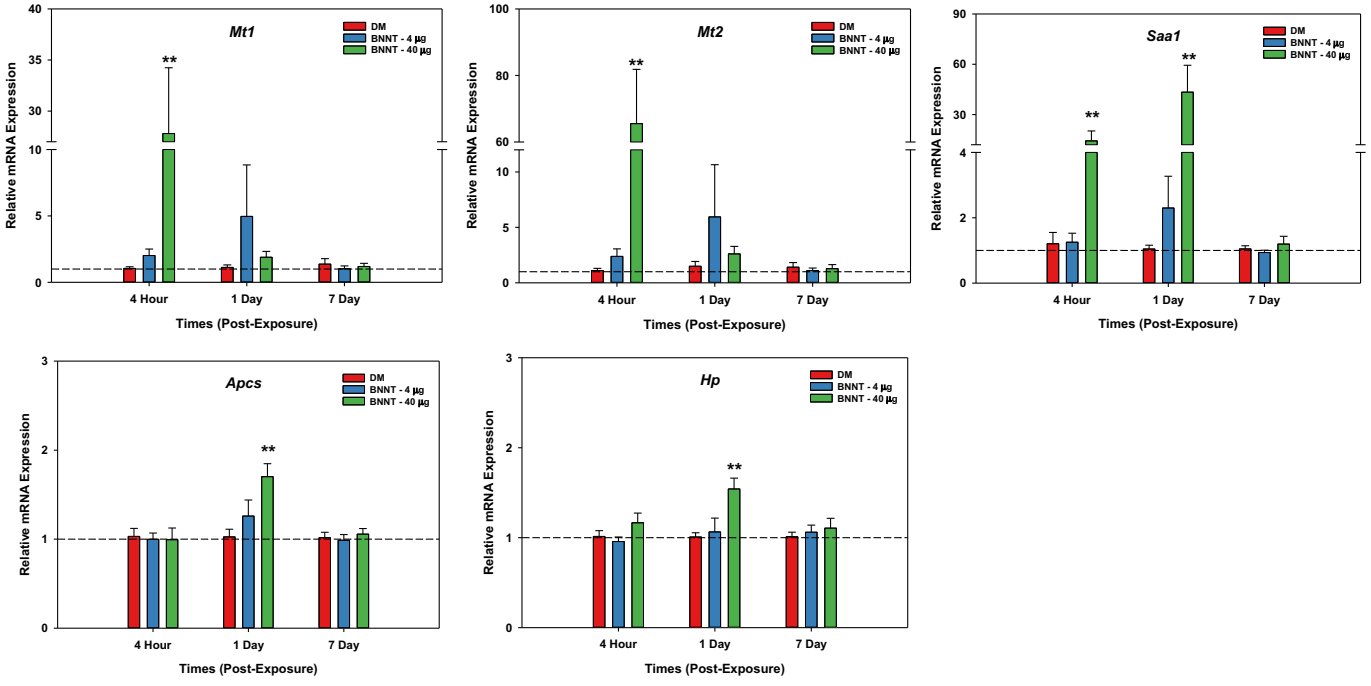

Fig. 10. Gene expression in liver tissue. Relative mRNA expression of Serum Amyloid A1 (*Saa1*), Serum Amyloid P-Component (*Apcs*), metallothionein 1 (*Mt1*), metallothionein 2 (*Mt2*), haptoglobin (*Hp*), relative to DM control at 4 h, 1 d, and 7 d post-exposure (n = 8 per group per time point). **Significantly different from all groups, $p < 0.01$; *significantly different from all groups, $p < 0.05$.

nanotubes) and time course (up to 2 mo post-exposure). In the comparisons discussed below, it should be noted that the purity of BNNT used in this study was around ~50–60% nanotubes as compared to > 99% nanotubes in the MWCNT studies. The findings in this study showed that changes were observed in the lung primarily only at the high dose of BNNT exposure in terms of lung injury and inflammation. These effects were greatest at the earlier time points' post-exposure, which is consistent with the acute findings of Kodali et al. (2017). In the current study, lung injury was demonstrated by increased LDH activity in the BAL fluid (Fig. 3), beginning at 4 h post-exposure, persisting until 7 d post-exposure, then resolving over time. Kodali et al. (2017) also performed an acute toxicity comparison between BNNT used in the current study and MWCNT-7, a more toxic form of MWCNT (El-Gazzar et al., 2019; Horie et al., 2019), at the same dose of 40 μg per mouse. Their study showed that the same BNNT as in the present study also significantly increased LDH, as well as IL-1β and IL-18, when compared to control but this difference was significantly less than that of MWCNT-7 at 1 d post-exposure when compared on a total particle mass basis. Additionally, they showed that BNNT caused an increase in reactive oxygen species in cells and this effect was also lower than that induced by MWCNT. It is important to note that the nanotube content of the two samples in that study differed significantly with the BNNT sample being approximately half that of the MWCNT sample.

In the present study, inflammation was measured as increased BAL cellular influx to the lung (neutrophils and eosinophils). Neutrophil influx was present at early time points in the high dose BNNT group and peaked at 1 d post-exposure (Fig. 5B), agreeing with the largest induction of proinflammatory cytokines IL-6, KC, MCP-1, MIP-1α, and MIP-2 (CXCL-2) in BAL fluid (Fig. 4). Eosinophil influx was also observed in the high dose BNNT group at early time points, with the greatest effect at 7 d post-exposure (Fig. 5C), which corresponded with the induction of IL-5 and eotaxin in BAL fluid (Fig. 4), proteins involved in eosinophils recruitment in inflammation and irritant response. In addition to increased inflammatory and immune markers in the BAL fluid of high dose BNNT exposed mice, gene expression in the lung followed a similar pattern as BAL protein analysis, with increased mRNA expression of genes encoding proinflammatory factors, IL-6 (*Il6*), macrophage MIP-2 (*Ccl2*), MCP-1 (*Cxcl2*) and macrophage-derived chemokine (MDC) (*Ccl22*) peaking at the early time points (Fig. 8); although gene expression decreased over time, there was still a significant elevation over control at 2 mo. *Il-5* and *Ccl11* gene expressions in the lung tissue were also increased at 4 h post-exposure (Fig. 8), which was consistent with the increased protein levels in BAL fluid.

The cytokines measured in the BAL fluid provided a partial analysis of the innate immune response induced by BNNT, but whether this is part of the overall inflammatory response, a specific irritancy response, or part of a greater immune response indicative of whether the material could contribute to allergic responses was not investigated. Although boron has not been commonly associated with the potential for allergic sensitization or exacerbation of existing asthmatic responses, many metals/metalloids with negligible allergic potential exhibit enhanced immunogenicity in nanoscale formulations (Roach et al., 2019a). In this context, the simultaneous expansion of B-cell populations within the LN, increase in BAL eosinophil number, and elevated levels of prototypical Th2 cytokines in the BAL fluid of the BNNT high dose group at 7 days suggests that exposure may have potential implications for respiratory allergy. Collectively, these observations indicate that the nature of the local inflammatory response may prime the lungs for allergic sensitization following subsequent encounters with aeroallergens—a response which has been well-characterized by incorporating other engineered nanomaterials and ultrafine particles into asthma models (Li et al., 2016; Meldrum et al., 2017). For example, when administered by oropharyngeal aspiration 1 day prior to sensitization with ovalbumin, the local inflammatory responses caused by a single exposure to NiONP, CuONP, and ZnONP were shown to promote the development of allergic airway responses and magnify Th2-polarized immune reactivity (Roach et al., 2019b; Horie et al., 2015, 2016). Comparatively, repeated lung exposure to some nanomaterials prior to sensitization has been shown to attenuate Th2 involvement in asthmatic responses. Repeated dosing of SiO_2NP, Fe_2O_3NP, and MWCNT prior to sensitization has been shown to cause decreases in lung eosinophil burden, Th2 cytokine production, and IgE levels following allergen challenge *in vivo* (Ban et al., 2013; Han et al., 2011; Ihrie et al., 2019). Similar studies have also been performed with MWCNT, and similarly, there are also conflicting data on whether the allergic response is increased or attenuated (Ihrie et al., 2019; Nygaard et al., 2009; Park et al., 2009; Ronzani et al., 2014).

Th2 polarization has also been implicated in development of fibrosis (Dong and Ma, 2016). The histopathological results in the present study showed that no alveolar wall thickening, and epithelial cell changes such as hypertrophy or hyperplasia were present in any groups (Table 1). Only a minimal level of inflammatory cell infiltration in the high dose BNNT group was observed and persisted up to 2 mo post-exposure (Table 1). The greatest degree of damage was observed at 7 d, which can be seen in Fig. 5A which demonstrate and area of high accumulation of macrophages containing BNNT. No pulmonary effects were observed at the low dose of BNNT exposure. This study was designed to replicate that of collaborators, Porter et al. (Porter et al., 2010), that examined a similar dose-response time course study of MWCNT-7. They found that MWCNT-7 exposure rapidly caused histopathological evidence of pulmonary inflammation and damage, which peaked at 7 d post-exposure and persisted over time at the 40 μg dose. Porter et al. (Porter et al., 2010) also found that MWCNT-7 exposure caused rapid development of lung fibrosis as early as 7 d post-exposure, which was not found in BNNT exposure in the present study. Again, it is important to note that the BNNT sample in the present study was only ~50–60% nanotubes, with a lower aspect ratio than MWCNT-7 following dispersion. Other studies of MWCNT at an equivalent dose of nanotubes as the BNNT high dose in this study, which would be ~20 of MWCNT, have also shown that MWCNT is likely more toxic (Porter et al., 2010; Ronzani et al., 2012; Han et al., 2010). Collectively, these studies cover three different sources of MWCNT with different dimensions and surface properties; however, all studies at doses of 20–25 μg MWCNT showed increased inflammation indicated by increased LDH, neutrophil response and cytokine levels. Additionally, Ronzani et al. (2012), demonstrated increased collagen indicative of fibrosis and Porter et al. (2010), showed fibrosis development and persistent inflammatory response at 2 mo post-exposure. In the current study, BNNT pathology related to inflammation peaked at 7 d; however, the responses had resolved by the 2 mo time point.

It is important to note that the current study only examined effects up to 2 mo post-exposure. The development of fibrotic disease for a less potent material than MWCNT-7 could take longer. As mentioned earlier, Th2 cytokines are increased and this has been associated with development of fibrosis (Dong and Ma, 2016). Additionally, in the present study, gene expression of osteopontin (OPN; *Spp1* gene), also known as secreted phosphoprotein 1 (SPP1), was significantly induced at 7 d, and remained elevated at 1 mo and 2 mo post-exposure in the high dose group. OPN is a potential marker of the development of lung diseases including fibrosis (Dong and Ma, 2017, 2019; Khaliullin et al., 2015, 2017) and cancer (Zhao et al., 2018). Khaliullin et al. (2017) demonstrated that induction of OPN expression was important in initiating the cellular mechanisms of pulmonary fibrosis induced by single-walled carbon nanotubes (SWCNT) in mice. Dong and Ma's study (Dong and Ma, 2017) also showed that OPN was highly induced throughout the study from 1 d to 56 d in the lungs of C57BL/6 J mice exposed to MWCNTs, and played critical roles in promoting fibrosis development from MWCNT exposure. Although the commercial grade BNNT sample used here caused an increase in the OPN gene expression throughout the time course, no pathology in the lung was present at 2 mo. In addition, EDM (Fig. 6) images showed that BNNT macrophage particle load was lower in BAL and in lung tissues at the later time

points relative to the 7 d time point. T Lung burden analysis showed that approximately 50% of the BNNT sample had been cleared over the time course; however, the majority of that clearance occurred between 7 d and 1 mo followed by a slowing of the clearance rate. Differences in clearance pattern and rate may account for differences in MWCNT-induced fibrosis, where clearance may be slower or impeded depending on the form of MWCNT (Mercer et al., 2013a; Shinohara et al., 2016).

The current study also investigated a set of systemic indices of toxicity following pulmonary exposure to BNNT, which was transient and minimal. The greatest responses in liver (Fig. 10) and blood cell profiles (Fig. 9B and C) were observed at 4 h and 1 d post-exposure in the high dose BNNT group. These responses did not persist beyond the early time points post-exposure, with resolution over time. Serum amyloid A (SAA) is secreted during the acute phase of inflammation and SAA1 isoform is expressed and induced principally in liver during inflammation (Uhlar and Whitehead, 1999). At 4 h and 1 d post-exposure, *Saa1* gene expression was highly induced, which was consistent with the acute inflammation induced by the high dose of BNNT (Fig. 10). Metallothionein (MT) is a family of protein playing a role in the protection against metal toxicity and oxidative stress. The expression of *Mt1* and *Mt2* is induced by several factors including metals, some drugs, oxidative stress, and inflammatory mediators (Szrok et al., 2016; Vasak and Meloni, 2011). In the current study, increased expression of *Mt1* and *Mt2* genes in the liver was observed at 4 h post-exposure in the high dose of BNNT group (Fig. 10), which could be due to the generation of oxidative stress by the BNNT exposure since MT plays a protective role *via* the scavenging of radical species. In a previous study, Kodali et al. showed that BNNT induced a dose-dependent increase in oxidative stress both in human monocytic THP-1 cells and in C57BL/6 J mice after a 24 h exposure (Kodali et al., 2017), which could explain why the expression of *Mt1* and *Mt2* was increased as an early response in the current study. These effects had resolved by 7 d post-exposure. The results in this study suggested that oxidative stress could be one of the possible mechanisms of acute toxicity observed following BNNT exposure.

In general, the BNNT sample investigated here did not cause persistent toxicity in the lung or systemically. Despite the dimensional structure similarities between the prepared BNNT and MWCNT, BNNT may not be as potent as some of the more toxic forms of MWCNT. In relationship to MWCNT-induced inflammation, some studies have shown that pulmonary inflammation was more persistent following respiratory exposure to MWCNT (Aiso et al., 2010; Han et al., 2010; Kobayashi et al., 2010, 2017; Morimoto et al., 2012; Muller et al., 2005; Porter et al., 2010), whereas others show varying degrees of resolution in inflammation over time (Knudsen et al., 2019; Poulsen et al., 2016; Silva et al., 2014). In the current study, the pulmonary inflammation following BNNT exposure was transient with resolution over time in the high dose group. This difference from some MWCNT responses could be due to the impurity of the BNNT samples used in the present study. As mentioned above, the sample used here represents an occupational exposure in a facility; however, that exposure is to a complex particle which contains only ~50–60% nanotubes, whereas most of the MWCNT studies have a much higher percentage of nanotubes. Additionally, toxicity may be attributed to other differences in physicochemical properties, such as difference in degree of aggregation/entanglement, surface area, surface chemistry, length and diameter after dispersion preparation, and biopersistence. For example, Poulson et al., showed differing outcomes for MWCNT that varied in surface area and surface oxidation state (Poulsen et al., 2016). Others have also shown surface modification alters MWCNT toxicity (Hussain et al., 2016; Sager et al., 2014). The BNNT used in this study had no measurable metal contaminants associated with the surface, and boron compounds have been demonstrated by others to be involved in the mediation of oxidative stress and inflammation (Donoiu et al., 2018; Pizzorno, 2015), which may account for some differences in toxicity as compared to some of the more toxic MWCNT.

Importantly, BNNT is a high aspect ratio nanomaterial, as is MWCNT, and toxicity related physicochemical properties that are also important to the fiber paradigm may apply to these materials (Donaldson et al., 2011; Poland et al., 2009). The important physicochemical properties in this toxicity paradigm are diameter, length, and biopersistence, which in turn is dependent on a number of properties including durability of the material. The BNNT sample used in the present study was manufactured to have dimensions of 5 nm wide and up to 200 μm long, but the dispersion preparation effectively shortened the length to an average of ~0.6–1.6 μm, which means that the clearance of the prepared BNNT may occur more rapidly than longer nanotubes and toxicity may also be lower. Very few *in vivo* studies of BNNT are available to assess this; however, although not directly related to pulmonary pathology of the fiber paradigm, *in vitro* studies in human cell lines have demonstrated the importance of aspect ratio in potential BNNT toxicity (Ciofani et al., 2014; Horvath et al., 2011). Ciofani et al. (2014) performed biocompatibility tests using the same BNNTs as used in the work of Horvath et al. (2011), but with a shorter length (~1.5 μm long) due to a homogenization/sonication treatment for dispersion in gum Arabic aqueous solutions. Their results showed that no toxicity up to 20 μg/ml were observed in human endothelial and neuron-like cells, which indicated that ultra-pure short BNNTs may be suitable for *in vitro* biomedical applications up, whereas Horvath et al. (2011) showed detrimental effects in lung and embryonic kidney cell cultures at concentration of approximate 2 μg/ml with the same BNNT of longer length (Horvath et al., 2011). In comparison, the sample used in the current study and in Kodali et al. (2017) had a lower percentage of BNNT and was shortened by the sample preparation, but also had a smaller diameter leading to an aspect ratio that falls between the studies of Ciofani et al. (2014) and Horvath et al. (2011). The findings related to BNNT toxicity in Kodali et al. (2017) using THP-1 monocytes were more in line with the findings of Horvath et al. (2011); additionally, the MWCNT-7 (49 nm in diameter and 3.86 μm in length) used in the study by Kodali et al. (2017) had a much higher purity and aspect ratio than BNNT and were more toxic at higher doses than the BNNT.

Differences in aspect ratio and biopersistence are also important factors in MWCNT toxicity (Shannahan and Brown, 2015), and may account for differences between MWCNT and BNNT as well. A number of studies have shown that shorter MWCNT tended to induce less persistent pulmonary inflammation than long MWCNT (Chen et al., 2014; Hamilton Jr. et al., 2013; van Berlo et al., 2014; Wang et al., 2013). Knudsen et al. (2019) showed that degree of entanglement, diameter, and metal contaminants determine adverse pulmonary outcomes following MWCNT exposure, and also demonstrated the importance of these factors in the persistence of the materials in the lung. The straighter, needle-like and longer MWCNT showed stronger toxic effects and carcinogenic potency than the more bent, curved and shorter MWCNT (Catalan et al., 2016; Rittinghausen et al., 2014). A short, thin, entangled type of MWCNT was reported to induce more pulmonary inflammation than a longer and thicker fiber-like MWCNT type, but only the longer and thicker MWCNT induced fibrosis (Poulsen et al., 2015). The BNNT sample in this study is morphologically more similar to entangled material, and has a lower aspect ratio once prepared for aspiration, which may partially account for the lack of fibrotic response in the lung. In terms of biopersistence in the lung, the present study is the first study to examine a time course following pulmonary exposure to BNNT. Over the time course ~50% of the material was cleared from the lung with the highest rate of clearance between 7 d and 1 mo. Very little clearance was observed between 1 mo and 2 mo; however, toxicity resolved to a great degree over time. Pulmonary clearance and biopersistence in the lung are also dependent on a number of different particle properties as has been demonstrated in studies with various forms of MWCNT reviewed by Kuempel et al. (2017). Some forms of MWCNT have been shown to persist in the lung after one or two years of long-term exposure in mice or rats (Kasai et al., 2016; Knudsen et al.,

2019; Sargent et al., 2014). There are currently no studies available for comparison of BNNT samples with varying material properties to determine if the same factors are critical in the clearance of BNNT following pulmonary exposure. Further studies are needed to fully elucidate toxicity associated with BNNT exposures.

5. Conclusions and future research directions

This is the first *in vivo* time course study examining toxicity of a BNNT material following pulmonary exposure in a mouse model. The findings in the present study suggested that the high aspect ratio material BNNT caused acute injury and inflammation in the lung as early as 4 h post-exposure. The effects peaked at 7 d but resolved to varying degrees over time up to 2 mo post-exposure. The exposure did not progress to disease in the lung, such as fibrosis. Only the high dose of BNNT caused increased lung injury and inflammation, whereas the low dose preparation in this study did not induce any effects in the lung. The conclusion pertained to only this preparation of nanotubes as the BNNT sample used in this study was not 100% BNNT and the aspect ratio of the material was significantly reduced in particle preparation, which might result in a different effects and pathology in the lung. Based on the findings in this study, there are several research needs are indicated. Further studies are needed on material with a higher percentage of nanotubes and on hBN itself in the nanoparticle form to determine if structure or chemical components will impact the toxicity profile of BNNT, particularly whether a higher percentage of tube in the materials alter the fibrotic response. These investigations are currently underway. Additionally, the early Th2 and eosinophilic response warrant further examination of the potential to induce or alter allergic response. The study also did not investigate strain- or gender-related differences, and these are important factors to take into consideration in risk assessment and hazard evaluation.

CRediT authorship contribution statement

Xing Xin:Conceptualization, Methodology, Formal analysis, Visualization, Writing - original draft.**Mark Barger**:Investigation, Visualization.**Katherine A. Roach**:Formal analysis, Investigation, Visualization.**Lauren Bowers**:Investigation.**Aleksandr B. Stefaniak**:Methodology, Investigation.**Vamsi Kodali**:Investigation.**Eric Glassford**:Resources, Investigation.**Kevin L. Dunn**:Resources, Investigation.**Kevin H. Dunn**:Resources, Investigation.**Michael Wolfarth**:Investigation.**Sherri Friend**:Investigation.**Stephen S. Leonard**:Methodology.**Michael Kashon**:Formal analysis.**Dale W. Porter**:Conceptualization.**Aaron Erdely**:Conceptualization.**Jenny R. Roberts**:Conceptualization, Methodology, Supervision, Project administration, Writing - review & editing.

Declaration of competing interest

The authors declare that they have no known competing financial interests or personal relationships that could have appeared to influence the work reported in this paper.

Acknowledgements

The authors would like to acknowledge Dr. Eileen Kuempel for her expertise and assistance with the lung deposition modeling using the MPPD software.

Funding statement

This work was supported by the National Institute for Occupational Safety and Health (intramural grant number 931043T).

Disclaimer

The findings and conclusions in this report are those of the authors and do not necessarily represent the official position of the National Institute for Occupational Safety and Health, Centers for Disease Control and Prevention. Mention of brand name does not constitute product endorsement.

References

Aiso, S., Yamazaki, K., Umeda, Y., Asakura, M., Kasai, T., Takaya, M., Toya, T., Koda, S., Nagano, K., Arito, H., Fukushima, S., 2010. Pulmonary toxicity of intratracheally instilled multiwall carbon nanotubes in male Fischer 344 rats. Ind. Health 48, 783–795.

ASTM, 2002. Standard Test Method for Metal Powder Specific Surface Area by Physical Adsorption. B922-02. ASTM International, West Conshohocken, PA.

ASTM, 2008. Standard Test Method for Metal Powder Skeletal Density by Helium or Nitrogen Pycnometry. B923. ASTM International, West Conshohocken, PA.

ATSDR, 2010. Toxicological Profile for Boron.

Ban, M., Langonne, I., Huguet, N., Guichard, Y., Goutet, M., 2013. Iron oxide particles modulate the ovalbumin-induced Th2 immune response in mice. Toxicol. Lett. 216, 31–39.

Bishop, L., Cena, L., Orandle, M., Yanamala, N., Dahm, M.M., Birch, M.E., Evans, D.E., Kodali, V.K., Eye, T., Battelli, L., Zeidler-Erdely, P.C., Casuccio, G., Bunker, K., Lupoi, J.S., Lersch, T.L., Stefaniak, A.B., Sager, T., Afshari, A., Schwegler-Berry, D., Friend, S., Kang, J., Siegrist, K.J., Mitchell, C.A., Lowry, D.T., Kashon, M.L., Mercer, R.R., Geraci, C.L., Schubauer-Berigan, M.K., Sargent, L.M., Erdely, A., 2017. In vivo toxicity assessment of occupational components of the carbon nanotube life cycle to provide context to potential health effects. ACS Nano 11, 8849–8863.

Cal, T., Bucurgat, U.U., 2019. In vitro investigation of the effects of boron nitride nanotubes and curcumin on DNA damage. DURA, J. Pharm. Sci. 27, 203–218.

Catalan, J., Siivola, K.M., Nymark, P., Lindberg, H., Suhonen, S., Jarventaus, H., Koivisto, A.J., Moreno, C., Vanhala, E., Wolff, H., Kling, K.I., Jensen, K.A., Savolainen, K., Norppa, H., 2016. In vitro and in vivo genotoxic effects of straight versus tangled multi-walled carbon nanotubes. Nanotoxicology 10, 794–806.

Chen, X., Wu, P., Rousseas, M., Okawa, D., Gartner, Z., Zettl, A., Bertozzi, C.R., 2009. Boron nitride nanotubes are noncytotoxic and can be functionalized for interaction with proteins and cells. J. Am. Chem. Soc. 131, 890–891.

Chen, T., Nie, H., Gao, X., Yang, J., Pu, J., Chen, Z., Cui, X., Wang, Y., Wang, H., Jia, G., 2014. Epithelial-mesenchymal transition involved in pulmonary fibrosis induced by multi-walled carbon nanotubes via TGF-beta/Smad signaling pathway. Toxicol. Lett. 226, 150–162.

Chopra, N.G., Luyken, R.J., Cherrey, K., Crespi, V.H., Cohen, M.L., Louie, S.G., Zettl, A., 1995. Boron nitride nanotubes. Science 269, 966–967.

Ciofani, G., Danti, S., D'Alessandro, D., Moscato, S., Menciassi, A., 2010. Assessing cytotoxicity of boron nitride nanotubes: interference with the MTT assay. Biochem. Biophys. Res. Commun. 394, 405–411.

Ciofani, G., Danti, S., Genchi, G.G., D'Alessandro, D., Pellequer, J.L., Odorico, M., Mattoli, V., Giorgi, M., 2012. Pilot in vivo toxicological investigation of boron nitride nanotubes. Int. J. Nanomedicine 7, 19–24.

Ciofani, G., Danti, S., Nitti, S., Mazzolai, B., Mattoli, V., Giorgi, M., 2013. Biocompatibility of boron nitride nanotubes: an up-date of in vivo toxicological investigation. Int. J. Pharm. 444, 85–88.

Ciofani, G., Del Turco, S., Rocca, A., de Vito, G., Cappello, V., Yamaguchi, M., Li, X., Mazzolai, B., Basta, G., Gemmi, M., Piazza, V., Golberg, D., Mattoli, V., 2014. Cytocompatibility evaluation of gum Arabic-coated ultra-pure boron nitride nanotubes on human cells. Nanomedicine (Lond) 9, 773–788.

Donaldson, K., Murphy, F., Schinwald, A., Duffin, R., Poland, C.A., 2011. Identifying the pulmonary hazard of high aspect ratio nanoparticles to enable their safety-by-design. Nanomedicine (Lond) 6, 143–156.

Dong, J., Ma, Q., 2016. In vivo activation of a T helper 2-driven innate immune response in lung fibrosis induced by multi-walled carbon nanotubes. Arch. Toxicol. 90, 2231–2248.

Dong, J., Ma, Q., 2017. Osteopontin enhances multi-walled carbon nanotube-triggered lung fibrosis by promoting TGF-beta1 activation and myofibroblast differentiation. Part Fibre Toxicol 14, 18.

Dong, J., Ma, Q., 2019. In vivo activation and pro-fibrotic function of NF-kappaB in fibroblastic cells during pulmonary inflammation and fibrosis induced by carbon nanotubes. Front. Pharmacol. 10, 1140.

Donoiu, I., Militaru, C., Obleaga, O., Hunter, J.M., Neamtu, J., Bita, A., Scorei, I.R., Rogoveanu, O.C., 2018. Effects of boron-containing compounds on cardiovascular disease risk factors - a review. J. Trace Elem. Med. Biol. 50, 47–56.

El-Gazzar, A.M., Abdelgied, M., Alexander, D.B., Alexander, W.T., Numano, T., Iigo, M., Naiki, A., Takahashi, S., Takase, H., Hirose, A., Kannno, J., Elokle, O.S., Nazem, A.M., Tsuda, H., 2019. Comparative pulmonary toxicity of a DWCNT and MWCNT-7 in rats. Arch. Toxicol. 93, 49–59.

EPA, 1996. Method 6010B-Inductively Coupled Plasma-Atomic Emission Spectrometry.

EPA, 2004. Toxicological Review of Boron and Compounds (CAS No. 7440–42-8): In Support of Summary Information on the Integrated Risk Information System (IRIS).

Golberg, D., Bando, Y., Tang, C.C., Zhi, C.Y., 2007. Boron nitride nanotubes. Adv. Mater. 19, 2413–2432.

Hamilton Jr., R.F., Wu, Z., Mitra, S., Shaw, P.K., Holian, A., 2013. Effect of MWCNT size, carboxylation, and purification on in vitro and in vivo toxicity, inflammation and

lung pathology. Part Fibre Toxicol 10, 57.
Han, S.G., Andrews, R., Gairola, C.G., 2010. Acute pulmonary response of mice to multi-wall carbon nanotubes. Inhal. Toxicol. 22, 340–347.
Han, B., Guo, J., Abrahaley, T., Qin, L., Wang, L., Zheng, Y., Li, B., Liu, D., Yao, H., Yang, J., Li, C., Xi, Z., Yang, X., 2011. Adverse effect of nano-silicon dioxide on lung function of rats with or without ovalbumin immunization. PLoS One 6, e17236.
Horie, M., Stowe, M., Tabei, M., Kuroda, E., 2015. Pharyngeal aspiration of metal oxide nanoparticles showed potential of allergy aggravation effect to inhaled ovalbumin. Inhal. Toxicol. 27, 181–190.
Horie, M., Stowe, M., Tabei, M., Kuroda, E., 2016. Metal ion release of manufactured metal oxide nanoparticles is involved in the allergic response to inhaled ovalbumin in mice. Occup Dis Environ Med 4, 17.
Horie, M., Tabei, Y., Sugino, S., Fukui, H., Nishioka, A., Hagiwara, Y., Sato, K., Yoneda, T., Tada, A., Koyama, T., 2019. Comparison of the effects of multiwall carbon nanotubes on the epithelial cells and macrophages. Nanotoxicology 13, 861–878.
Horvath, L., Magrez, A., Golberg, D., Zhi, C., Bando, Y., Smajda, R., Horvath, E., Forro, L., Schwaller, B., 2011. In vitro investigation of the cellular toxicity of boron nitride nanotubes. ACS Nano 5, 3800–3810.
Hubbs, A.F., Sargent, L.M., Porter, D.W., Sager, T.M., Chen, B.T., Frazer, D.G., Castranova, V., Sriram, K., Nurkiewicz, T.R., Reynolds, S.H., Battelli, L.A., Schwegler-Berry, D., McKinney, W., Fluharty, K.L., Mercer, R.R., 2013. Nanotechnology: toxicologic pathology. Toxicol. Pathol. 41, 395–409.
Hussain, S., Ji, Z., Taylor, A.J., DeGraff, L.M., George, M., Tucker, C.J., Chang, C.H., Li, R., Bonner, J.C., Garantziotis, S., 2016. Multiwalled carbon nanotube functionalization with high molecular weight hyaluronan significantly reduces pulmonary injury. ACS Nano 10, 7675–7688.
ICRP, 1994. Human respiratory tract model for radiological protection. A report of a Task Group of the International Commission on Radiological Protection. Ann. ICRP 24, 1–482.
Ihrie, M.D., Taylor-Just, A.J., Walker, N.J., Stout, M.D., Gupta, A., Richey, J.S., Hayden, B.K., Baker, G.L., Sparrow, B.R., Duke, K.S., Bonner, J.C., 2019. Inhalation exposure to multi-walled carbon nanotubes alters the pulmonary allergic response of mice to house dust mite allergen. Inhal. Toxicol. 31, 192–202.
Jakubinek, M.B., Ashrafi, B., Martinez-Rubi, Y., Guan, J., Rahmat, M., Kim, K.S., Dénommée, S., Kingston, C.T., Simard, B., 2019. Chapter 5 - boron nitride nanotube composites and applications. In: Nanotube Superfiber Materials. William Andrew Applied Science Publisher, pp. 91–111.
Janzen, E.G., Blackburn, B.J., 1968. Detection and identification of short-lived free radicals by an electron spin resonance trapping technique. J. Am. Chem. Soc. 90, 5909–5910.
Kasai, T., Umeda, Y., Ohnishi, M., Mine, T., Kondo, H., Takeuchi, T., Matsumoto, M., Fukushima, S., 2016. Lung carcinogenicity of inhaled multi-walled carbon nanotube in rats. Part Fibre Toxicol 13, 53.
Khaliullin, T.O., Shvedova, A.A., Kisin, E.R., Zalyalov, R.R., Fatkhutdinova, L.M., 2015. Evaluation of fibrogenic potential of industrial multi-walled carbon nanotubes in acute aspiration experiment. Bull. Exp. Biol. Med. 158, 684–687.
Khaliullin, T.O., Kisin, E.R., Murray, A.R., Yanamala, N., Shurin, M.R., Gutkin, D.W., Fatkhutdinova, L.M., Kagan, V.E., Shvedova, A.A., 2017. Mediation of the single-walled carbon nanotubes induced pulmonary fibrogenic response by osteopontin and TGF-beta1. Exp. Lung Res. 43, 311–326.
Kim, J.H., Pham, T.V., Hwang, J.H., Kim, C.S., Kim, M.J., 2018. Boron nitride nanotubes: synthesis and applications. Nano Converg 5, 17.
Knudsen, K.B., Berthing, T., Jackson, P., Poulsen, S.S., Mortensen, A., Jacobsen, N.R., Skaug, V., Szarek, J., Hougaard, K.S., Wolff, H., Wallin, H., Vogel, U., 2019. Physicochemical predictors of multi-walled carbon nanotube-induced pulmonary histopathology and toxicity one year after pulmonary deposition of 11 different multi-walled carbon nanotubes in mice. Basic Clin Pharmacol Toxicol 124, 211–227.
Kobayashi, N., Naya, M., Ema, M., Endoh, S., Maru, J., Mizuno, K., Nakanishi, J., 2010. Biological response and morphological assessment of individually dispersed multi-wall carbon nanotubes in the lung after intratracheal instillation in rats. Toxicology 276, 143–153.
Kobayashi, N., Izumi, H., Morimoto, Y., 2017. Review of toxicity studies of carbon nanotubes. J. Occup. Health 59, 394–407.
Kodali, V.K., Roberts, J.R., Shoeb, M., Wolfarth, M.G., Bishop, L., Eye, T., Barger, M., Roach, K.A., Friend, S., Schwegler-Berry, D., Chen, B.T., Stefaniak, A., Jordan, K.C., Whitney, R.R., Porter, D.W., Erdely, A.D., 2017. Acute in vitro and in vivo toxicity of a commercial grade boron nitride nanotube mixture. Nanotoxicology 11, 1040–1058.
Kuempel, E.D., Jaurand, M.C., Moller, P., Morimoto, Y., Kobayashi, N., Pinkerton, K.E., Sargent, L.M., Vermeulen, R.C., Fubini, B., Kane, A.B., 2017. Evaluating the mechanistic evidence and key data gaps in assessing the potential carcinogenicity of carbon nanotubes and nanofibers in humans. Crit. Rev. Toxicol. 47, 1–58.
Lee, C.H., Bhandari, S., Tiwari, B., Yapici, N., Zhang, D., Yap, Y.K., 2016. Boron nitride nanotubes: recent advances in their synthesis, functionalization, and applications. Molecules 21.
Li, N., Georas, S., Alexis, N., Fritz, P., Xia, T., Williams, M.A., Horner, E., Nel, A., 2016. A work group report on ultrafine particles (American Academy of Allergy, Asthma & Immunology): why ambient ultrafine and engineered nanoparticles should receive special attention for possible adverse health outcomes in human subjects. J. Allergy Clin. Immunol. 138, 386–396.
Meldrum, K., Guo, C., Marczylo, E.L., Gant, T.W., Smith, R., Leonard, M.O., 2017. Mechanistic insight into the impact of nanomaterials on asthma and allergic airway disease. Part Fibre Toxicol 14, 45.
Mercer, R.R., Scabilloni, J.F., Hubbs, A.F., Battelli, L.A., McKinney, W., Friend, S., Wolfarth, M.G., Andrew, M., Castranova, V., Porter, D.W., 2013a. Distribution and fibrotic response following inhalation exposure to multi-walled carbon nanotubes. Part Fibre Toxicol 10, 33.
Mercer, R.R., Scabilloni, J.F., Hubbs, A.F., Wang, L., Battelli, L.A., McKinney, W., Castranova, V., Porter, D.W., 2013b. Extrapulmonary transport of MWCNT following inhalation exposure. Part Fibre Toxicol 10, 38.
Morimoto, Y., Hirohashi, M., Ogami, A., Oyabu, T., Myojo, T., Todoroki, M., Yamamoto, M., Hashiba, M., Mizuguchi, Y., Lee, B.W., Kuroda, E., Shimada, M., Wang, W.N., Yamamoto, K., Fujita, K., Endoh, S., Uchida, K., Kobayashi, N., Mizuno, K., Inada, M., Tao, H., Nakazato, T., Nakanishi, J., Tanaka, I., 2012. Pulmonary toxicity of well-dispersed multi-wall carbon nanotubes following inhalation and intratracheal instillation. Nanotoxicology 6, 587–599.
Muller, J., Huaux, F., Moreau, N., Misson, P., Heilier, J.F., Delos, M., Arras, M., Fonseca, A., Nagy, J.B., Lison, D., 2005. Respiratory toxicity of multi-wall carbon nanotubes. Toxicol. Appl. Pharmacol. 207, 221–231.
NIOSH, 2007. NIOSH Pocket Guide to Chemical Hazards.
Nygaard, U.C., Hansen, J.S., Samuelsen, M., Alberg, T., Marioara, C.D., Løvik, M., 2009. Single-walled and multi-walled carbon nanotubes promote allergic immune responses in mice. Toxicol. Sci. 109, 113–123.
Park, E.-J., Cho, W.-S., Jeong, J., Yi, J., Choi, K., Park, K., 2009. Pro-inflammatory and potential allergic responses resulting from B cell activation in mice treated with multi-walled carbon nanotubes by intratracheal instillation. Toxicology 259, 113–121.
Pizzorno, L., 2015. Nothing boring about boron. Integr Med (Encinitas) 14, 35–48.
Poland, C.A., Duffin, R., Donaldson, K., 2009. High aspect ratio nanoparticles and the fibre pathogenicity paradigm. In: Sahu, S.C., Casciano, D.A. (Eds.), Nanotoxicity: From In Vivo and In Vitro Models to Health Risks. John Wiley & Sons, Ltd, pp. 61–79.
Porter, D., Sriram, K., Wolfarth, M., Jefferson, A., Schwegler-Berry, D., Andrew, M.E., Castranova, V., 2008. A biocompatible medium for nanoparticle dispersion. Nanotoxicology 2, 144–154.
Porter, D.W., Hubbs, A.F., Mercer, R.R., Wu, N., Wolfarth, M.G., Sriram, K., Leonard, S., Battelli, L., Schwegler-Berry, D., Friend, S., Andrew, M., Chen, B.T., Tsuruoka, S., Endo, M., Castranova, V., 2010. Mouse pulmonary dose- and time course-responses induced by exposure to multi-walled carbon nanotubes. Toxicology 269, 136–147.
Poulsen, S.S., Saber, A.T., Williams, A., Andersen, O., Kobler, C., Atluri, R., Pozzebon, M.E., Mucelli, S.P., Simion, M., Rickerby, D., Mortensen, A., Jackson, P., Kyjovska, Z.O., Molhave, K., Jacobsen, N.R., Jensen, K.A., Yauk, C.L., Wallin, H., Halappanavar, S., Vogel, U., 2015. MWCNTs of different physicochemical properties cause similar inflammatory responses, but differences in transcriptional and histological markers of fibrosis in mouse lungs. Toxicol. Appl. Pharmacol. 284, 16–32.
Poulsen, S.S., Jackson, P., Kling, K., Knudsen, K.B., Skaug, V., Kyjovska, Z.O., Thomsen, B.L., Clausen, P.A., Atluri, R., Berthing, T., Bengtson, S., Wolff, H., Jensen, K.A., Wallin, H., Vogel, U., 2016. Multi-walled carbon nanotube physicochemical properties predict pulmonary inflammation and genotoxicity. Nanotoxicology 10, 1263–1275.
Rittinghausen, S., Hackbarth, A., Creutzenberg, O., Ernst, H., Heinrich, U., Leonhardt, A., Schaudien, D., 2014. The carcinogenic effect of various multi-walled carbon nanotubes (MWCNTs) after intraperitoneal injection in rats. Part Fibre Toxicol 11, 59.
Roach, K.A., Stefaniak, A.B., Roberts, J.R., 2019a. Metal nanomaterials: immune effects and implications of physicochemical properties on sensitization, elicitation, and exacerbation of allergic disease. J. Immunotoxicol. 16, 87–124.
Roach, K.A., Anderson, S.E., Stefaniak, A.B., Shane, H.L., Kodali, V., Kashon, M., Roberts, J.R., 2019b. Surface area- and mass-based comparison of fine and ultrafine nickel oxide lung toxicity and augmentation of allergic response in an ovalbumin asthma model. Inhal. Toxicol. 31, 299–324.
Ronzani, C., Spiegelhalter, C., Vonesch, J.-L., Lebeau, L., Pons, F., 2012. Lung deposition and toxicological responses evoked by multi-walled carbon nanotubes dispersed in a synthetic lung surfactant in the mouse. Arch. Toxicol. 86, 137–149.
Ronzani, C., Casset, A., Pons, F., 2014. Exposure to multi-walled carbon nanotubes results in aggravation of airway inflammation and remodeling and in increased production of epithelium-derived innate cytokines in a mouse model of asthma. Arch. Toxicol. 88, 489–499.
Sager, T.M., Wolfarth, M.W., Andrew, M., Hubbs, A., Friend, S., Chen, T.H., Porter, D.W., Wu, N., Yang, F., Hamilton, R.F., Holian, A., 2014. Effect of multi-walled carbon nanotube surface modification on bioactivity in the C57BL/6 mouse model. Nanotoxicology 8, 317–327.
Salvetti, A., Rossi, L., Iacopetti, P., Li, X., Nitti, S., Pellegrino, T., Mattoli, V., Golberg, D., Ciofani, G., 2015. In vivo biocompatibility of boron nitride nanotubes: effects on stem cell biology and tissue regeneration in planarians. Nanomedicine (Lond) 10, 1911–1922.
Sargent, L.M., Porter, D.W., Staska, L.M., Hubbs, A.F., Lowry, D.T., Battelli, L., Siegrist, K.J., Kashon, M.L., Mercer, R.R., Bauer, A.K., Chen, B.T., Salisbury, J.L., Frazer, D., McKinney, W., Andrew, M., Tsuruoka, S., Endo, M., Fluharty, K.L., Castranova, V., Reynolds, S.H., 2014. Promotion of lung adenocarcinoma following inhalation exposure to multi-walled carbon nanotubes. Part Fibre Toxicol 11, 3.
Schmittgen, T.D., Livak, K.J., 2008. Analyzing real-time PCR data by the comparative C(T) method. Nat. Protoc. 3, 1101–1108.
Shannahan, J.H., Brown, J.M., 2015. Multiwalled carbon nanotube-induced pulmonary fibrogenesis. In: Otsuki, T., Yoshioka, Y., Holian, A. (Eds.), Biological Effects of Fibrous and Particulate Substances, pp. 149–162.
Shinohara, N., Nakazato, T., Ohkawa, K., Tamura, M., Kobayashi, N., Morimoto, Y., Oyabu, T., Myojo, T., Shimada, M., Yamamoto, K., Tao, H., Ema, M., Naya, M., Nakanishi, J., 2016. Long-term retention of pristine multi-walled carbon nanotubes in rat lungs after intratracheal instillation. J. Appl. Toxicol. 36, 501–509.
Silva, R.M., Doudrick, K., Franzi, L.M., TeeSy, C., Anderson, D.S., Wu, Z., Mitra, S., Vu, V., Dutrow, G., Evans, J.E., Westerhoff, P., Van Winkle, L.S., Raabe, O.G., Pinkerton, K.E., 2014. Instillation versus inhalation of multiwalled carbon nanotubes: exposure-related health effects, clearance, and the role of particle characteristics. ACS Nano 8, 8911–8931.

Smith, M.W., Jordan, K.C., Park, C., Kim, J.W., Lillehei, P.T., Crooks, R., Harrison, J.S., 2009. Very long single- and few-walled boron nitride nanotubes via the pressurized vapor/condenser method. Nanotechnology 20, 505604.
Stone, K.C., Mercer, R.R., Gehr, P., Stockstill, B., Crapo, J.D., 1992. Allometric relationships of cell numbers and size in the mammalian lung. Am. J. Respir. Cell Mol. Biol. 6, 235–243.
Szrok, S., Stelmanska, E., Turyn, J., Bielicka-Gieldon, A., Sledzinski, T., Swierczynski, J., 2016. Metallothioneins 1 and 2, but not 3, are regulated by nutritional status in rat white adipose tissue. Genes Nutr. 11, 18.
Tiano, A.L., Park, C., Lee, J.W., Luong, H.H., Gibbons, L.J., Chu, S., Applin, S., Gnoffo, P., Lowther, S., Kim, H.J., Danehy, P.M., Inman, J.A., Jones, S.B., Kang, J.H., Sauti, G., Thibeault, S.A., Yamakov, V., Wise, K.E., Su, J., Fay, C.C., 2014. Boron nitride nanotube: synthesis and applications. SPIE Proc. 9060, 1–19.
Uhlar, C.M., Whitehead, A.S., 1999. Serum amyloid A, the major vertebrate acute-phase reactant. Eur. J. Biochem. 265, 501–523.
van Berlo, D., Wilhelmi, V., Boots, A.W., Hullmann, M., Kuhlbusch, T.A., Bast, A., Schins, R.P., Albrecht, C., 2014. Apoptotic, inflammatory, and fibrogenic effects of two different types of multi-walled carbon nanotubes in mouse lung. Arch. Toxicol. 88, 1725–1737.
Vasak, M., Meloni, G., 2011. Chemistry and biology of mammalian metallothioneins. J. Biol. Inorg. Chem. 16, 1067–1078.
Wang, P., Nie, X., Wang, Y., Li, Y., Ge, C., Zhang, L., Wang, L., Bai, R., Chen, Z., Zhao, Y., Chen, C., 2013. Multiwall carbon nanotubes mediate macrophage activation and promote pulmonary fibrosis through TGF-beta/Smad signaling pathway. Small 9, 3799–3811.
Zhao, H., Chen, Q., Alam, A., Cui, J., Suen, K.C., Soo, A.P., Eguchi, S., Gu, J., Ma, D., 2018. The role of osteopontin in the progression of solid organ tumour. Cell Death Dis. 9, 356.
Zhi, C.Y., Bando, Y., Tang, C.C., Xie, R., Sekiguchi, T., Golberg, D., 2005. Perfectly dissolved boron nitride nanotubes due to polymer wrapping. J. Am. Chem. Soc. 127, 15996–15997.